Applications of MXene-Containing Polypyrrole Nanocomposites in Electrochemical Energy Storage and Conversion

Gbolahan Joseph Adekoya, Oluwasegun Chijioke Adekoya, Rotimi Emmanuel Sadiku, Yskandar Hamam, and Suprakas Sinha Ray*

Cite This: *ACS Omega* 2022, 7, 39498−39519

Read Online

ACCESS | Metrics & More | Article Recommendations

ABSTRACT: The atomically thick two-dimensional (2D) materials are at the forefront of revolutionary technologies for energy storage devices. Due to their fascinating physical and chemical features, these materials have gotten a lot of attention. They are particularly appealing for a wide range of applications, including electrochemical storage systems, due to their simplicity of property tuning. The MXene is a type of 2D material that is widely recognized for its exceptional electrochemical characteristics. The use of these materials in conjunction with conducting polymers, notably polypyrrole (PPy), has opened new possibilities for lightweight, flexible, and portable electrodes. Therefore, herein we report a comprehensive review of recent achievements in the production of MXene/PPy nanocomposites. The structural–property relationship of this class of nanocomposites was taken into consideration with an elaborate discussion of the various characterizations employed. As a result, this research gives a narrative explanation of how PPy interacts with distinct MXenes to produce desirable high-performance nanocomposites. The effects of MXene incorporation on the thermal, electrical, and electrochemical characteristics of the resultant nanocomposites were discussed. Finally, it is critically reviewed and presented as an advanced composite material in electrochemical storage devices, energy conversion, electrochemical sensors, and electromagnetic interference shielding.
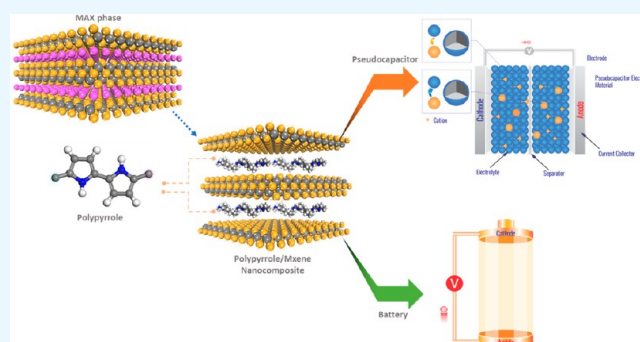
1. INTRODUCTION

Nanomaterials have a vital part in the development of energy storage technologies, which are critical for human life.[1,2] Owing to their fascinating physical and chemical features, these materials have gotten a lot of attention. They include monoelemental single-layer crystals, also known as Xenes (e.g., borophene, graphene, silicene, and phosphorene), functionalized monoelemental single-layer crystal derivatives, also known as Xanes (e.g., borophane and graphane), MXenes (e.g., Ti_2CO_2, $Ti_3C_2T_x$, and Ti_3C_2), transition metal halides (e.g., CrI_3), semiconductors and insulators of groups III−V (e.g., boron nitride), transition metal dichalcogenides (e.g., $TaSe_2$ and MoS_2), organic−inorganic hybrid perovskites (e.g., Pb-$(C_4H_9NH_3)_2I_4$), and post-transition metal chalcogenides (e.g., GaS and GaSe).[3] Among these nanomaterials, MXenes have recently piqued academic curiosity.[4−10]

MXenes are a class of 2D inorganic compounds that are made up of a few atoms' thick layers of transition metal nitrides, carbides, or carbonitrides. They have a general formula of $M_{n+1}X_nT_x$ ($n = 1, 2, 3$) where M is an early transition metal such as Ti or Sc and X is either carbon or nitrogen. T_x represents the surface terminations, such as −O, −OH, and/or −F.[11] More than 30 members of this class of material have been experimentally realized with several possibilities predicted theoretically.[12,13] They exhibit several desirable features, such as small band gaps, metallic conductivity, and a plastic layer surface. MXenes are highly investigated for energy storage applications due to their 2D nanostructures.[4−10,14] Their electrochemical performance is largely influenced by their structural configuration, surface chemistry, morphology, and composition. For instance, the use of the $Ti_3C_2T_x$ MXene as an anode material for the rechargeable battery has proven to improve battery performance by shortening ion-diffusion lengths, providing active interfaces, and enhancing in-plane carriers. The potential use of MXene for energy storage includes ultracapacitors, and metal-ion rechargeable batteries such as

lithium-ion batteries, lithium-sulfur batteries, and sodium-ion batteries.[6,10]

Unlike Xene, the functional groups terminating on the structure of MXene are usually developed during synthesis and do not negatively affect the electrical conductivity of the structure. Instead, they impact stability in the structure, and their contributing properties correlate with the M element, both of which ultimately improve the electronic and optical properties of the material.[15] MXenes are obtained from layered MAX phases (Figure 1(a)), which are a class of two-dimensional
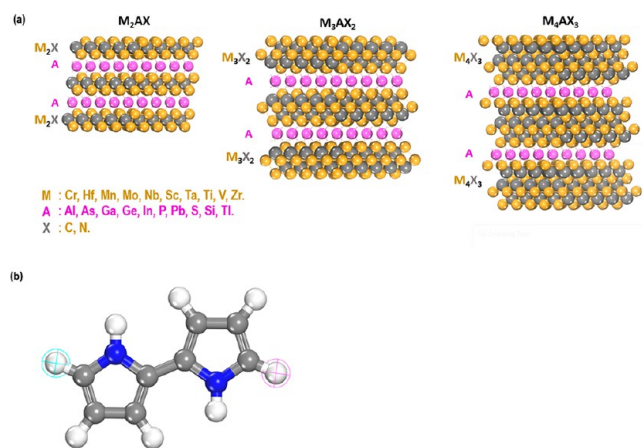

Figure 1. 3D structural representation of (a) MAX phase materials and (b) the repeating unit of polypyrrole.

materials with layered hexagonal structures.[16] They are synthesized by a top-down selective etching of the A-layer in MAX phases or similar precursors. This process employs strong etching solutions of the fluoride ion (F^-) such as hydrofluoric acid (HF), ammonium bifluoride (NH_4HF_2), and a mixture of hydrochloric acid (HCl) and lithium fluoride (LiF).[17] They can be classified based on their crystal structure. These include mono solid solution M-element type, M-element type, ordered double M-element type, and vacancy ordering type. They are particularly appealing for various applications, including electrochemical storage systems, due to their ease of property tuning.[7-10,18-24]

In combination with conducting polymers, MXene offers exceptional reinforcing properties due to the surface terminal group present in its structure.[12,25] Moreover, polymeric materials serving as the matrix for MXene are an excellent candidate for producing wearable and flexible electronic devices. As a result, the MXene/polymer nanocomposite offers significant advantages ranging from versatility, compatibility, and cost to high-performance products.[26] One of the prominent conducting polymers that has received substantial attention in recent years as a suitable matrix for MXene is polypyrrole (PPy).[27-29,29-33] The 3D chemical structure of PPy is presented in Figure 1(b). Owing to its high electrical conductivity, the polymer is widely used for lightweight, flexible, and cheap energy storage applications, specifically for supercapacitors and batteries.[28] For instance, Zhu et al.[35] and Wu et al.[36] hybridize PPy chains with MXene to produce a high-performing freestanding and flexible ultracapacitor. Similarly, Dan et al.[34] established a facile approach via in situ polymerizations to develop the PPy nanosphere/Ti_3C_2-MXene (PPy/Ti_3C_2) nanocomposite as an electrode in supercapacitor electrodes, whereas Jian et al.[32] used one-step coelectrodeposition to

prepare a nanocomposite of MXene and PPy. Due to the termination groups, 2D $Ti_3C_2T_x$-MXene nanosheets worked as a core polymer, and pyrrole monomer radical cations (Py^+) slowly polymerized on the surface and layer space of the 2D MXene nanosheets. Yan et al.,[33] on the other hand, demonstrated the use of a PPy−MXene nanocomposite to coat textile-based flexible energy storage devices. Beyond energy storage, the PPy−MXene nanocomposite has been reported to be used as a biosensor. Zhou et al.[35] fabricated a ternary nanocomposite by including phosphomolybdic acid (PMo_{12}) in the composite to boost the electrochemical detection of osteopontin, OPN, by an impedimetric aptamer biosensor.

The MXene/PPy nanocomposite is quickly gaining research attention for energy storage; there is still a lot to understand comparatively about the mechanism and properties of the inclusion of MXenes in the PPy matrix. This gap incites this current paper. Moreover, while the capacitive energy storage use of the PPy/MXene nanocomposite was reviewed by Ezika et al.,[36] this work intends to examine the most recent breakthroughs in the synthesis, characterization, and properties of the MXene/PPy nanocomposite as a further step in this field, with a focus on the electrochemical energy storage and conversion applications. Therefore, the first section of this paper gives a narrative description of how PPy interacts with different MXenes to make desirable high-performance nanocomposites. Then MXene's incorporation impact on the thermal, electrical, and electrochemical properties of the resulting nanocomposites was studied. Finally, its application as an energy storage material in electrochemical storage devices (batteries and supercapacitors), energy conversion (electrocatalysis), electrochemical sensors, and electromagnetic interference shielding is discussed, followed by a highlight on the prospective outlook of this noble class of material.

2. SYNTHESIS OF MXENE/PPY NANOCOMPOSITES

2.1. Overview of the Synthesis of PPy. PPy is an attractive conductive polymer for energy storage applications owing to its high electrical conductivity, processability, redox potential, eco-friendliness, and stability.[27] It can be prepared through a chemical[37-41] or electrochemical polymerization route.[42] The chemical polymerization of PPy involves the coupling of radical cations in which the oxidized pyrrole monomer gives rise to a radical cation at the start of the polymerization process. The oxidation of pyrrole can be facilitated with the use of oxidants (such as $K_2Cr_2O_7$, $FeCl_3$, $CuCl_2$, and $KMnO_4$), halogens (e.g., chlorine, bromine, and iodine), and strong acids.[43] This is followed by deprotonation of the coupled radical cations to yield bipyrrole. The resulting bipyrrole reoxidizes and couples with a different oxidized bipyrrole to form an oligomer. The process proceeds in that format of oxidation, coupling, and deprotonation to eventually produce PPy. Afshin et al.[42] employed a solvent-free deposition to synthesize highly conductive PPy films with a conductivity of 180 $S·cm^{-1}$, although this mechanism is different from the proposed chemical polymerization of pyrrole in an aqueous medium, particularly in water, due to its scalability and environmental benignity. Based on this, Yuefei et al.[41] created a high crystalline PPy with a conductivity of 0.3 $S\ cm^{-1}$ by using the interface area of the two solutions. Figure 2 ((a → b → d → e → f → g) and (a → c → d → e → f → g)) shows the two main possible chemical polymerization routes for synthesizing PPy.[44]

For precise PPy film preparation, electrochemical polymerization is the technique of choice. This method produces pure
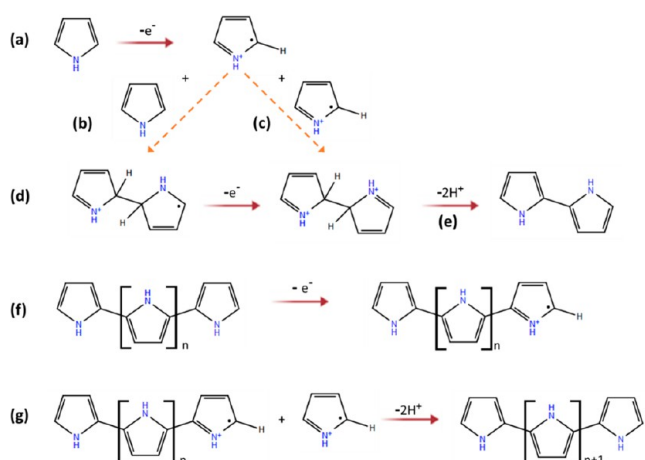
deposited on an electrode substrate (e.g., glassy carbon, tin, or indium-tin oxide (ITO) coated glass and gold) in the presence of electrolyte using several electrochemical methods such as galvanostatic (constant current), potentiostat (constant-potential), and potentiodynamic (linear potential scanning) techniques. In addition to the intrinsic conductivity resulting from the conjugated structure of PPy, electrical conduction can be incited in the polymer through the redox process. The process can yield either a p-doped (oxidation) or n-doped (reduction) polymer followed by the insertion of delocalized positive or negative ions, resulting in enhanced ionic transport. Therefore, to synthesize PPy through electrochemical polymerization, the pyrrole monomers are dissolved in an aqueous electrolyte, followed by oxidation at the electrode by applying an anodic potential. The oxidized pyrrole produces a radical cation which reacts with another monomer in the solution to yield an oligomer. This reaction continues in this fashion to finally produce oxidized PPy. Several mechanisms, such as Diaz's, Kim's, Pletcher's, and Reynold's, have been proposed to explain the electrochemical polymerization of pyrrole monomers to PPy. Figure 2 (a → c → d → e → f → g) illustrates the electropolymerization mechanism of PPy as depicted by Diaz and the team.[45,46] Although the synthesized PPy possesses lower oxidative potential compared

Figure 2. Schematic representation of the two major synthesis routes for chemical polymerization of PPy (a → b → d → e → f → g) and (a → c → d → e → f → g). The electropolymerization mechanism of PPy as depicted by Diaz et al. (a → c → d → e → f → g).

PPy with controlled film morphology and thickness, unlike chemical polymerization. As such, the monomer is electro-
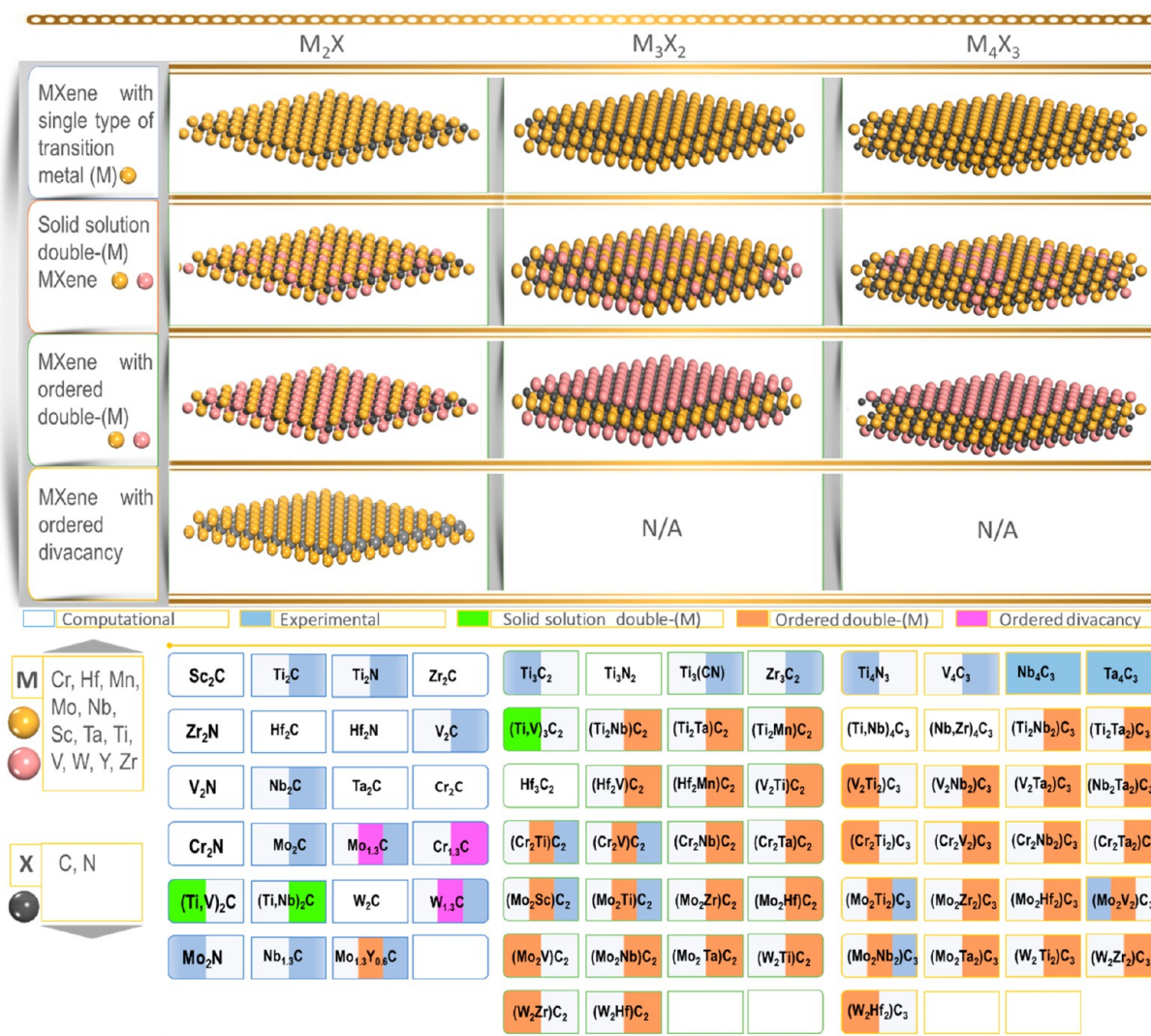

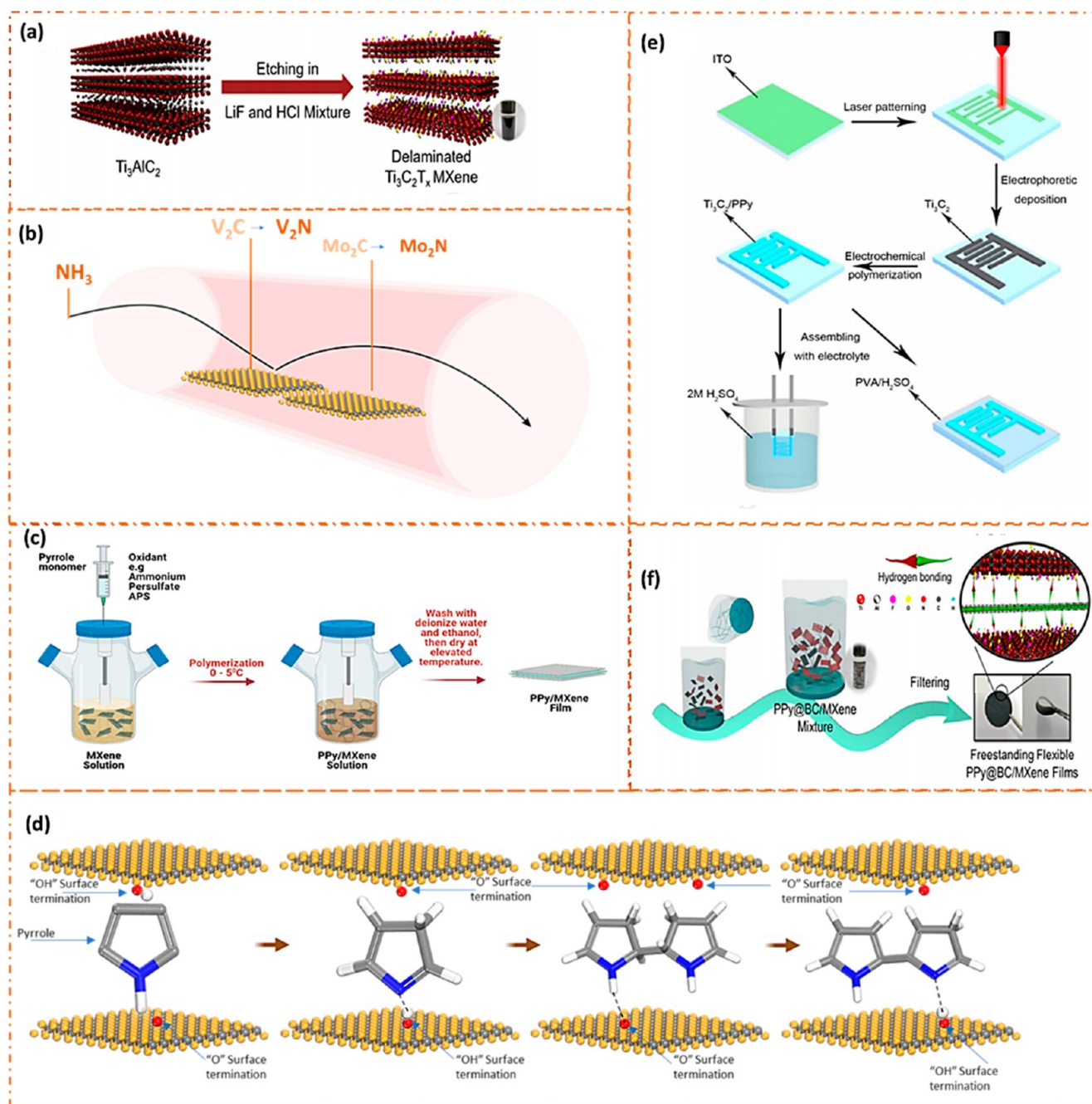**Figure 3.** Different types of MXenes synthesized theoretically and experimentally.

Figure 4. Schematic representation of the (a) synthesis of $Ti_3C_2T_x$ through selective etching of Ti_3AlC_2 phase material using a solution of LiF and HCl. Reprinted with permission from ref 70. Copyright 2021, Springer Nature. (b) Ammoniation technique of carbide MXenes (Mo_2CT_x and V_2CT_x) to the synthesis of 2D transition metal nitrides at high temperatures. (c) In situ polymerization of the polypyrrole/MXene nanocomposite. Reprinted with permission from ref 69. Copyright 2020, Elsevier Science Ltd. (d) Dimerization of β-protonated pyrrole monomers in the MXene interlayer. Reprinted with permission from ref 69. Copyright 2020, Elsevier Science Ltd. (e) Electrophoretic deposition and electrochemical polymerization approach to building a planar supercapacitor based on Ti_3C_2/PPy interdigital electrodes. Reprinted with permission from ref 69. Copyright 2020, Elsevier Science Ltd. (f) The solution fabrication process of PPy@BC and $Ti_3C_2T_x$ to produce freestanding flexible PPy@BC/MXene film. Reprinted with permission from ref 70. Copyright 2021, Springer Nature.

to its monomer, the reaction often proceeds simultaneously with the introduction of counteranions to balance the charge difference and increase its ionic conductivity.[46]

2.2. Overview of the Synthesis of MXene. MXenes are synthesized from precursor MAX phased materials using the chemical exfoliation method.[10,47,48] Figure 3 displays the list of MXenes realized experimentally and theoretically up until this publication.[10,48] To perform the synthesis, MAX phased materials are selectively etched with a suitable etchant such as

hydrogen fluoride (HF), fluoride salts (e.g., potassium fluoride (KF), sodium fluoride (NaF), and lithium fluoride (LiF)) (see Figure 4(a)), ammonium hydrogen bifluoride (NH_4HF_2), ammonium fluoride (NH_4F), and molten zinc chloride ($ZnCl_2$) salt. Figure 4(b) illustrates the ammoniation technique of carbide MXenes (Mo_2CT_x and V_2CT_x) to synthesize 2D transition metal nitrides at high temperatures. Different factors, such as the atomic number of the transition metal, surface defect, edge termination, and environmental impact, dictate the type of

etchant to be used. For instance, Naguib et al.[49] reported that there is a positive correlation between the atomic number of the transition metal and the etching period, as well as with the strength of the etchant. Meanwhile, using mild etchants such as fluoride salts yields MXene with fewer surface defects. Using etchants such as HF results in $-F$, $=O$, and $-OH$ edge termination. However, when NH_4HF_2 and $ZnCl_2$ are employed, the MXene obtained possesses suppressed $-F$ and $-Cl$ termination, respectively. Besides, $ZnCl_2$ not only produces fluoride-free etching but also is equally environmentally benign. So far, three methods of chemically exfoliating MAX phase material to synthesize MXene have been identified. These include wet chemical etching, molten salt etching, and electrochemical etching.[50,51] Details of the advances in the various methods have been comprehensively reviewed in ref 52.

2.3. Fabrication of PPy/MXene Nanocomposites. Several techniques are available for fabricating polymer/ MXene nanocomposites, including oxidative in situ polymerization, oxidant-free in situ polymerization, solution blending, etc.[25,53] However, in situ polymerization is the most used technique for PPy/MXene nanocomposites. The process requires the use of a monomer and initiator under reaction temperature.[54] Solution blending, on the other hand, has been seldomly used for the synthesis of MXene/PPy. With these methods, MXenes are either randomly dispersed in the matrix of PPy or dispersed in a structured order. The resulting composite often exhibits good interaction between the matrix and the inclusion. This is largely due to the excellent hydrophilicity of MXene and PPy.[25,55]

2.3.1. In Situ Oxidative Polymerization of PPy/MXene Nanocomposites. PPy/MXene nanocomposites can be synthesized through chemical[41,47,56] and electrochemical[57] polymerization at a controlled temperature. These methods are commonly used in the fabrication of a polymer nanocomposite due to the homogeneous dispersion of nanosheets in the polymer matrix.[58,59] Besides, these methods often result in a structured composite, excellent electrochemical properties, and good chemical bonding between the nanosheets of MXene and the PPy matrix.[60−62] The strong interfacial interaction between PPy chains and MXene nanosheets is promoted by several possible bonding mechanisms, including strong $\pi-\pi$ stacking and electrostatic interaction. Moreover, the electron-donating capability of PPy stimulates accelerated adsorption of the chains onto the electron-accepting surface of Ti_3C_2.[11,63] Therefore, in the chemical polymerization of the PPy/MXene nanocomposite, the exfoliated MXene nanosheets, the pyrrole monomer, and the required solvents such as *p*-toluenesulfonic acid and sodium *p*-toluenesulfonic are reacted at subambient temperature with or without oxidants such as ammonium persulfate (APS) and ferric chloric hexahydrate.[43,63] Figure 4(c) shows the in situ chemical polymerization process of MXene/PPy. To demonstrate the use of oxidative chemical polymerization, Wei et al.[34] employed a facile means to synthesize the PPy/Ti_3C_2 heterostructure nanocomposite through in situ polymerization. This method employs a solution of PVA, sodium *p*-toluenesulfonate, and pyrrole monomer dispersed in deionized water to grow PPy nanospheres on Ti_3C_2 nanosheets at subambient temperature. The reaction proceeded by vigorously stirring a solution of 0.1 g of PVA and 0.1 g of sodium *p*-toluenesulfonate in 40 mL of deionized (DI) water for half an hour. This was followed by adding 0.5 μL of pyrrole monomer and stirring for another half an hour in the reactor at low temperature. To initiate the reaction, an oxidant (1.14 g of APS)

was added in the aqueous form to the mixture in a dropwise fashion for 4 h while maintaining the temperature of the reaction at 1 °C. The solution of Ti_3C_2 was introduced to the reaction and further stirred for 8 h. The resulting composite was rinsed with DI water and anhydrous ethanol several times and freeze-dried for a day to obtain the Ti_3C_2/PPy nanocomposite. Similarly, Lei and colleagues[61] synthesized MXene/PPy under similar conditions to Wei and his co-worker.[34] However, $FeCl_3\cdot6H_2O$ was employed as the oxidant. The resulting nanocomposite was further annealed under an inert atmosphere for 2 h at 700, 800, and 900 °C for improved properties. Yang et al.[64] employed a comparable route to synthesize the MXene/PPy hybrid. After the polymerization was completed, they introduced a spraying technique to fabricate a ternary nanocomposite of MXene/PPy-PC film. The process was preceded by etching the PC film with an oxygen plasma cleaner for a minute to enhance its hydrophobicity. Then the aqueous solution of MXene/PPy that was synthesized earlier was sprayed onto the PC film at different volume ratios, and the resulting nanocomposite was dried at ambient temperature.[64] Meanwhile, Le and his team[65] slightly modified the oxidative chemical polymerization process by submerging a few cleaned nickel foam pieces into the pyrrole monomer solution with delaminated $Ti_3C_2T_x$. The solution was stirred for 24 h at ambient temperature. The MXene/PPy residue collected on the nickel foam was washed with DI water and ethanol and dried.[65] Along a similar path, Ding and his group[66] extended the synthesis of Ti_3C_2/PPy nanocomposites to include the SnO_2 nanocrystal to fabricate PPy/Ti_3C_2-SnO_2 for sodium storage.

2.3.2. Oxidant-Free in Situ Polymerization of the PPy/ MXene Nanocomposite. In some cases, oxidants are not used as initiators; however, as explained above, strong acid facilitates the oxidation of pyrrole. Thus, the acidic nature of MXene, particularly $Ti_3C_2T_x$, helps promote the polymerization of pyrrole.[43] For instance, Boota et al.[43] conducted an oxidant-free polymerization of pyrrole monomers intercalated between the stacked layers of MXene. The reaction was carried out by stirring the solution of d-$Ti_3C_2T_x$ and pyrrole vigorously at 1000 rpm at room temperature for 12 h. The resultant solution was vacuum filtered to collect the resulting nanocomposite. Similarly, Shao and a co-worker[67] synthesized PPy-d-$Ti_3C_2T_x$ by dissolving 10 mg of pyrrole monomer into 20 mL of DI water. The solution was stirred for 30 min, mixed with 10 mL of d-$Ti_3C_2T_x$ aqueous solution, and stirred for a day at ambient temperature. The precipitate was dried at 60 °C under a vacuum to obtain freestanding PPy-d-$Ti_3C_2T_x$ film.[67] Erol and colleagues[68] demonstrated the oxidation-free polymerization mechanisms of pyrrole on and in between Ti_3C_2 MXene surfaces and interlayers, respectively, using first-principles calculation. It was shown that the presence of $-O$ terminal atoms on the MXene surface improve pyrrole coordination and reduce the distance between the surface of the MXene and PPy monomer, whereas hydroxyl termination promotes polymerization of PPy by providing a source of proton for the β-carbon hydrogenation. Consequently, as shown in Figure 4(d), the oxidation-free polymerization of PPy between dual MXene surfaces proceeds with deprotonation of pyrrole and hydrogenation of the $-O$-terminated atoms on the MXene surface, which leads to strong hydrogen bonding between the MXene surface and the PPy monomer. Next, the resulting N-deprotonated pyrrole attracts protons from the $-OH$ terminal toward the β-carbons of pyrrole due to the lowered energy barrier of the monomer. The β-protonated pyrrole becomes spontaneous and can react with

Table 1. Preparation Methods for MXene/PPy Nanocomposites

species	technique	chemicals	remark	ref
Ti_3C_2/PPy	In situ polymerization	●0.1 g of PVA ●0.1 g of sodium *p*-toluene sulfonate ●deionized water ●anhydrous ethanol	Reaction took place at 1 °C for 4 h	34
MXene@PPy	In situ polymerization	●3.89 g of $FeCl_3 \cdot 6H_2O$	Reaction took place at 2 °C for 6 h	61
alk-Ti_3C_2/PPy	Chemical polymerization	●0.4 g of $FeCl_3 \cdot 6H_2O$	Reaction took place at room temperature for 4 h	60
PPy-coated MXene/ PMFF	Chemical polymerization	●0.87 g of $FeCl_3 \cdot 6H_2O$ ●0.5 g of *p*-toluene sulfonic acid (PTSA)	Reaction took place between 0 and 5 °C for 5 h	62
$Ti_3C_2T_x$/PPy	In situ polymerization	●without oxidant	Reaction took place at room temperature for 4 h and stirred at 1000 rpm	43
$Ti_3C_2T_x$/PPy	In situ polymerization	●APS as an oxidant ●PCV as a dispersant ●PVB as a binder	Reaction took place at 4 °C for 5 h and vacuum filtrated for 12 h	72
l-Ti_3C_2/PPy	Electrochemical polymerization	●*p*-toluene sulfonic acid (0.1 M) ●sodium *p*-toluene sulfonic (0.3 M) ●pyrrole monomer (300 μL)	Polymerized under constant voltage of 0.8 V versus Ag/AgCl	57
MXene/PPy	Electrochemical polymerization	●mg mL^{-1} LiCl ●0.2 M pyrrole	Polymerized under constant voltage of 0.8 V versus Ag/AgCl at 300 to 1800 s	32
PPy@BC/MXene	Solution processed	●deionized water	Continuously stirred for 4 h	70
$Ti_3C_2T_x$/PPy	Electrochemical polymerization	●M KNO_3 ●0.05 M pyrrole ●deionized water	Polymerized under constant voltage of 0.8 V using the chronoamperometry method	69
MXene@PPy	Chemical polymerization	●0.168 g of APS	Reaction took place between 0 and 2 °C for 5 h	64
MXene@PPy-PC	Spraying coating	●PC	Sprayed at a pressure and distance of 0.5 MPa and 5 cm	64
PPy-d-$Ti_3C_2T_x$	In situ polymerization	●deionized water	Continuously stirred at room temperature for 24 h	67
Ti_3C_2/PPy	In situ polymerization	●0.0879 g of APS	The reaction took place at 2 °C for 12 h	63
$Ti_3C_2T_x$@PPy	In situ polymerization	●without $FeCl_3 \cdot 6H_2O$ and methyl orange	Reaction lasted for 24 h at RT	65
$Ti_3C_2T_x$@PPy NW	Chemical polymerization	●2.5 g of $FeCl_3 \cdot 6H_2O$ ●0.3 g of dissolved methyl orange ●deionized water	Reaction took place at 0 °C for 24 h	65
PPy-SnO_2/Ti_3C_2	In situ interfacial growth	●40 mg of citric acid ●200 mL of pyrrole (PPy) monomer ●60 mg of NaClO ●30 mg of $SnCl_2$	-	66

diprotonated pyrrole or with a different β-protonated PPy with rearomatization.[68]

2.3.3. Electrochemical Polymerization of PPy/MXene Nanocomposites. Due to the intended use of PPy/MXene as electrode material, specifically, for energy application, most researchers often employ electrochemical polymerization to produce the PPy/MXene nanocomposite. In this process, both MXene and PPy are either electrochemically deposited individually on a substrate in a two-way process[57] or coelectrodeposited in a single step.[32] According to Zhu et al.,[57] in a two-way process, sonicated MXene solution is first deposited through electrophoretic means on FTO-coated glass at a bias potential of 15 V. The substrate employed serves as the working electrode. At the same time, Pt mesh is used as the counter electrode. After the process, the resulting MXene is rinsed and dried at elevated temperature under vacuum conditions for 12 h. Next, an aqueous solution of *p*-toluenesulfonic acid, sodium *p*-toluenesulfonic, and pyrrole monomer is then electrochemically polymerized onto the surface of the FTO-coated glass, having a deposition of l-Ti_3C_2 particles. This process is conducted under a constant voltage of 0.8 V versus Ag/AgCl for 600 s. The resulting

nanocomposite is rinsed and dried at elevated temperature under vacuum for 12 h to obtain a freestanding l-Ti_3C_2/PPy film. Similarly, Zhang et al.[69] prepared $Ti_3C_2T_x$/PPy using a chronoamperometry method; however, the film was deposited on a different substrate (ITO glass) with a solution of pyrrole monomer and KNO_3 (Figure 4e).

On the other hand, Jian and colleagues[32] demonstrated the electrochemical polymerization of PPy/MXene in a single step. The experiment proceeded by depositing a solution of $Ti_3C_2T_x$ and PPy under an inert atmosphere at a constant potential of 0.8 vs (Ag/AgCl)/V from 300 to 1800 s to obtain the MXene/PPy nanocomposite with a 3D carambola-like structure.

2.3.4. Solution Blending of PPy/MXene Nanocomposites. Just like for most polymer nanocomposites, the fabrication of MXene/PPy nanocomposites using the solution mixing method is equally possible. This wet process employs PPy solution instead of its monomer to prepare uniform thin nanocomposite films. In such a situation, the hydrophilic property of MXene, which is attributable to the presence of terminal hydroxyl functional groups on its structure, permits its rapid homogeneous dispersion in the aqueous PPy.[11] Then the interfacial interaction between PPy and MXene proceeds through
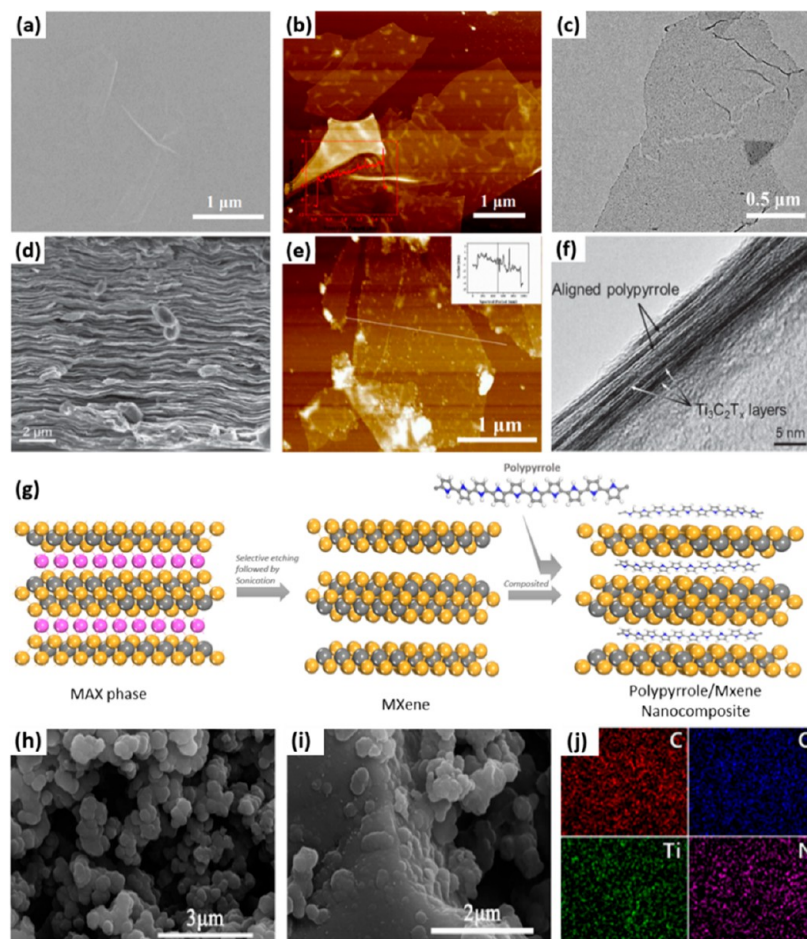
Figure 5. (a) SEM, (b) AFM, and (c) TEM micrographs of MXene. (d) SEM (cross-sectional view), (e) AFM, and (f) TEM (cross-sectional view) micrographs of MXene/PPy. (g) 3D atomic structural illustration of the process from the etching of MAX phase material to the fabrication of the MXene/PPy heterostructure nanocomposite. (h) SEM micrograph of polypyrrole nanospheres, (i) SEM micrograph of polypyrrole/MXene nanocomposites showing the agglomeration of PPy around MXene, and (j) C, O, Ti, and N elemental mapping for the MXene/PPy obtained by EDS. (a), (b), (c), (e), and (j) Reprinted with permission from ref 64. Copyright 2021, American Chemical Society. (d) and (f) Reprinted with permission from ref 43. Copyright 2015, John Wiley & Sons, Inc. (h) and (i) Reprinted with permission from ref 47. Copyright 2018, John Wiley & Sons, Inc.

hydrogen bonding due to the interaction between the NH group present in the PPy ring and terminal groups on the surface of MXene.[34,63] For instance, Song and colleagues[70] synthesized a ternary nanocomposite of PPy@bacterial cellulose/MXene. They initially prepared PPy with bacterial cellulose through in situ polymerization. Afterward, PPy@BC nanofibers obtained were dispersed in DI water to make 0.1 wt % of the PPy@BC solution. Similarly, a 0.2 wt % concentration of $Ti_3C_2T_x$ was prepared separately by dispersing delaminated $Ti_3C_2T_x$ nanoflakes in DI water. The two solutions were mixed at different mass ratios and stirred continuously for 4 h. The resulting suspension was vacuum filtered to produce PPy@BC/MXene films.[71] Figure 4(f) shows a schematic display of the facile solution processing of PPy@BC/MXene, whereas Table 1 summarizes the different preparatory methods for MXene/PPy nanocomposites.

3. CHARACTERIZATION OF PPY/MXENE NANOCOMPOSITES

Several characterization techniques have been employed to understand the interaction of MXene with PPy. This section provides an overview of the characteristic structural features and chemical compositions of MXene/PPy nanocomposites, which

promote their energy storage properties. The characteristics of nanocomposites are greatly influenced by their composition, particle size, interfacial contact, and other factors. Because MXene sheets have a high surface area, interfaces are crucial in influencing the characteristics of nanofilled materials. Owing to this interfacial area, a considerable volume of PPy around the nanosheet is impacted by the nanosheet surface and has characteristics that differ from the bulk polymer.

3.1. Morphology and Nanostructural Analysis of MXene/PPy Nanocomposites. Microscopy plays an essential role in material science by providing structural information and understanding the dynamics interplayed in combinatorial experimental designs involving the polymer matrix and nanofillers. Therefore, to describe the morphology and nanostructure of the MXene/PPy nanocomposite, several authors used various structural and spectroscopic techniques such as scanning electron microscopy (SEM), atomic force microscopy (AFM), transmission electron microscopy (TEM), energy-dispersive X-ray spectroscopy, and X-ray diffraction (XRD) to resolve structural information spanning the atomic to microscopic level of interfacial interactions. Microscopic studies reveal that the morphology of MXene, particularly Ti_3C_2, displays a wrinkled paper-like surface with potential sites for effective ion and electron transport. In addition, it can retain its layered

morphology after in situ polymerization of PPy and subsequent carbonization, indicating the selective etching of its precursor MAX phase material.[61,63] Figure 5(a−c) displays the SEM, AFM, and TEM micrographs of MXene, respectively. As such, the intercalation of homogeneous dispersion of MXene in PPy results in the heterostructure of the MXene/PPy nanocomposite having a porous cross-section that promotes the penetration of the electrolyte into the heterostructure during the charge/ discharge cycle.[57] Figure 5(d) and (f), respectively, shows the SEM and TEM cross-sectional view of the heterostructure of the MXene/PPy nanocomposite. At the same time, Figure 5(e) displays the AFM micrograph of the nanocomposite.[64] Besides, the introduction of MXene prevents the dense stacking of PPy, which enhances the electrochemical performance of the nanocomposite. The presence of PPy in the nanocomposite further expands its interlamellar spacing and thus provides an extra path for the movement of ionic species. Figure 5(g) illustrates the 3D structural transformation from the etching of MAX phase material to the intercalation of PPy chains with the layered MXene. Meanwhile, PPy exhibits a densely packed structure during electrochemical polymerization and can self-assemble into solid and uniform nanospheres with about 70−80 nm in diameter (Figure 5(h)).[34,47] In this state, the PPy nanospheres tend to agglomerate around or intertwine on the surface of the MXene layers due to several interactions, including π−π conjugate, hydrogen bonding, and electrostatic attraction (Figure 5(i)).[63,65] However, serious agglomeration is often prevented by the interlayered stacking of MXene.[34,63] The presence of uniformly dispersed MXene in the composite was further corroborated with EDS elemental mapping images in Figure 5(j), which shows the homogeneous distribution of C, O, Ti, and N elements.[61]

X-ray methods are frequently used to investigate the microscopic structure of polymer nanocomposites. The XRD technique is an effective analytical tool for identifying and characterizing crystalline materials. It is based on the elastic scattering of X-rays from structures with long-range order.[73] XRD patterns of MXene/PPy also buttress the sandwiched structure of PPy chains between the layered MXene. According to the XRD literature for the MXene/PPy nanocomposite, $Ti_3C_2T_x$ typically exhibits a characteristic pattern of five main peaks at (002), (006), (008), (0010), and (0012), which match the diffraction angles of ~9.1°, 18.3°, 27.8°, 34.6°, and 40.0°. The (002) peak is indicative of Ti_3C_2, while the rest of the peaks demonstrate characteristic features of 2D-layered structured material. Pristine PPy, on the other hand, exhibits a broad peak at diffraction angles ranging from 23.2° to 25.22°, which explains its amorphous nature. The peak of 1D nanostructured PPy is reported to appear at a higher diffraction angle (26°) than the bulk PPy.[65] When pyrrole is polymerized in the presence of MXene, specifically Ti_3C_2, there is a downward crystal plane shift in the diffraction angles of the (002) peak, with a corresponding increase in the d-spacing, which indicates the intercalation of the polymer.[34,47,61,63,65,70] Figure 6(a) demonstrates the XRD pattern of PPy, MXene, and MXene/PPy, exhibiting features of enhanced ion diffusion and charge transfer.

3.2. Surface Chemistry and Interfacial Structure of MXene/PPy Nanocomposites. Spectroscopic analyses such as FTIR, Raman, and XPS spectroscopy are commonly used to determine the chemical structure of MXene/PPy nanocomposites. FTIR studies reveal that the pyrrole and quinonoid ring vibrations in PPy are at 1571/1544 and 1455/1478 cm^{-1}, respectively.[34,63] Furthermore, pure PPy has a C−N stretching
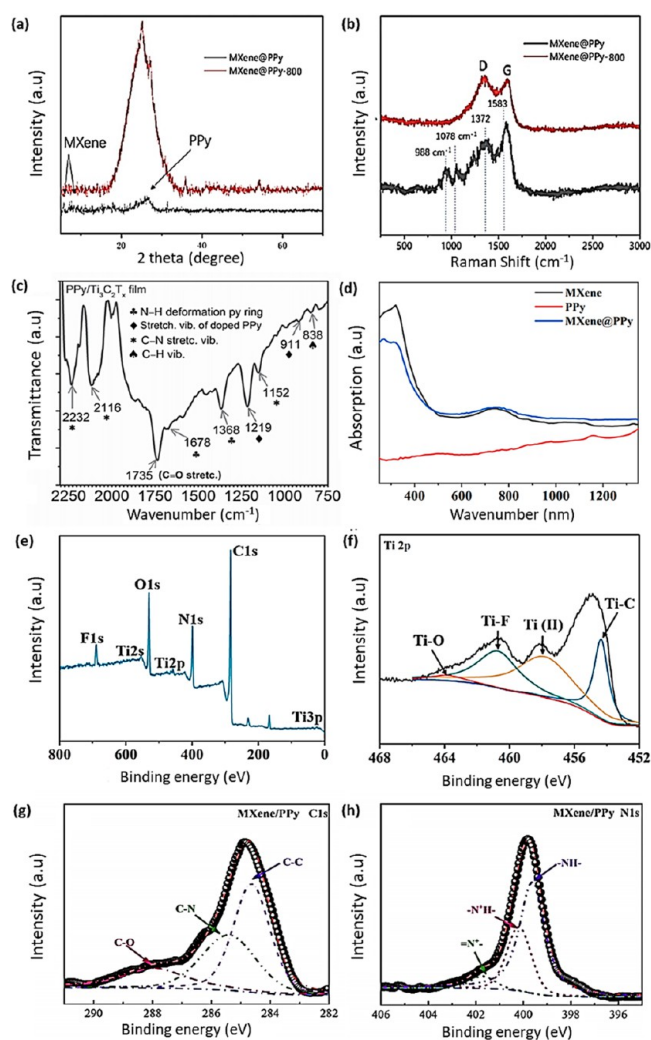
Figure 6. (a) XRD spectrum of the MXene/PPy nanocomposite and (b) Raman spectrum of the MXene/PPy nanocomposite. Reprinted from ref 61. This has been published under an open access Creative Common CC BY license. (c) FTIR spectrum of the MXene/PPy film. Reprinted with permission from ref 43. Copyright 2015 John Wiley & Sons, Inc. (d) UV−vis spectra of aqueous solutions of MXene, PPy, and the MXene@PPy hybrid. Reprinted with permission from ref 64. Copyright 2021, American Chemical Society. (e) XPS spectrum and (f) Ti 2p spectrum of MXene/PPy nanocomposites. Reprinted from ref 76. This has been published under an open access Creative Common CC BY license. (g) CI and (h) NI spectrum of MXene/PPy nano-composites. Reprinted with permission from ref 32. Copyright 2019, Elsevier Science Ltd.

vibration peak of 1321/1200 cm^{-1} and N−H stretching at 3683/ 1650 cm^{-1}, whereas from the FTIR spectrum of Ti_3C_2, the broad peaks at 3442 cm^{-1} and 1646/1628 cm^{-1} in the Ti_3C_2 nanosheets correlate to hydroxyl vibrations.[34,63] The combination of PPy and $Ti_3C_2T_x$ layers exhibits strong π−π interactions and hydrogen bond effects, which display characteristic bands that depend on factors such as the presence of additives and the mass content of the MXene and polymerization conditions.[47] Figure 6(b) depicts the FTIR spectrum of MXene/PPy nanocomposites. The polymerization of doped PPy in contact with $Ti_3C_2T_x$ without the use of dangerous oxidative agents was characterized using FTIR spectrometry. The stretching vibrations of the doped pyrrole ring were found to be connected with the adsorption bands at 1219 and 911 cm^{-1}, confirming the

synthesis of PPy in an oxidant-free pyrrole polymerization between 2D titanium carbide layers. The resulting MXene/PPy nanocomposite observed C−N and carbonyl stretching at FTIR bands of 2116 and 1735 cm^{-1}, respectively. The N−H deformation of the pyrrole ring is displayed by bands at 1678 and 1368 cm^{-1}. Meanwhile, the C−H vibrations within the pyrrole ring are detected at the absorption band of 838 cm^{-1}.[43] Increasing the volume fraction of Ti$_3$C$_2$ has been shown to impact the characteristic peaks of the Ti$_3$C$_2$/PPy nanocomposite by shifting the characteristic peaks of the nanocomposite to a lower wavenumber. This is attributed to interfacial contact between PPy nanospheres and Ti$_3$C$_2$ nanosheets.[34] Through a biotemplate synthesis of PPy@ bacterial cellulose, PPy nanoparticles were uniformly coated on BC nanofibers via strong interfacial contacts, resulting in distinctive FTIR peaks of C−O stretching vibration peaks of BC at 1157 and 1049 cm^{-1} to be shifted to 1118 and 1018 cm^{-1}, showing hydrogen bonding between BC and PPy. The C=C, C−N ring-stretching vibration, N−H in-plane bending vibration, and C−N in-plane deformation modes of PPy are ascribed to the evident peaks at 1533, 1437, 1648, and 1284 cm^{-1}, respectively, demonstrating that BC nanofibers are wrapped with PPy. The intercalation of PPy@BC nanofibers into Ti$_3$C$_2$T$_x$ layers creates a hierarchically packed nanofibrous structure with many electrochemical active sites. Still, the peaks corresponding to PPy@BC within the PBM composite film are present at 1645, 1533, 1435, 1284, 1120, and 1018 cm^{-1}, but the distinctive peak of N−H vibration moves from 862 to 840 cm^{-1} and becomes broader and stronger, showing the development of hydrogen bonding between Ti$_3$C$_2$T$_x$ and PPy.[70]

3.3. Raman. To investigate the structural information on Ti$_3$C$_2$T$_x$/PPy composites, Raman spectroscopy is commonly utilized as a suitable method. This method uses the inelastic scattering of monochromatic light, which is typically generated by a laser. The Raman effect occurs when laser light interacts with molecular vibrations, phonons, or other excitations in the system, causing the energy of re-emitted photons to be shifted up or down in relation to their initial monochromatic frequency. The shift reveals information on interfacial properties of polymer nanocomposites, including low-frequency vibrational, rotational, and other transitions in molecules.[74] Consequently, from the literature, the distinctive peaks of conductive PPy were reported to be seen in the spectrum of pure PPy and Ti$_3$C$_2$T$_x$/ PPy samples at around 1350 and 1590 cm^{-1}.[47] The creation of dications (bipolarons) is associated with Raman bands identified at 938, 1085, and 1261 cm^{-1}, while the one at 985 cm^{-1} is linked to a polaron structure when the mass concentration of Ti$_3$C$_2$T$_x$ in the composite is increased to double the mass content of PPy. Raman bands at 1590, 1320, 1042, 712, and 616 cm^{-1} are attributed to C=C stretching of two oxidized structures, inter-ring stretching, and C−C in-ring, C−H deformation, C−H wagging, and pyrrole ring torsion, respectively.[43] Furthermore, when the intensity ratio of the D/G bands, which is a measure of the defects in MXene's structure upon the intercalation of PPy, was explored, the obtained D band to G band (I_D/I_G) strength ratios of Ti$_3$C$_2$, PPy, and Ti$_3$C$_2$/PPy are 0.88, 0.82, and 0.98, respectively. Because the addition of PPy increases the edges/ defect, the I_D/I_G value of Ti$_3$C$_2$/PPy is higher than Ti$_3$C$_2$. The D and G bands of Ti$_3$C$_2$/PPy exhibit a minor shift toward low frequency when compared to Ti$_3$C$_2$, which is related to the strong interaction between the PPy and Ti$_3$C$_2$. C−C stretching and antisymmetric C−N stretching of the carbon skeleton are represented by the PPy bands at 1345 and 1565 cm^{-1},

respectively.[34] Figure 6(c) depicts the Raman spectrum of MXene/PPy. The D band at 1350 cm^{-1} and the G belt at 1570 cm^{-1} correspond to the sp^2 hybridization in-plane stretching vibration of carbon atoms and the defect of the carbon atom lattice, respectively.[61,63]

3.4. UV. One of the essential techniques for polymer nanocomposite investigation is IR spectroscopy, which studies the interaction of infrared light with matter. It clarifies the interaction between the polymer matrix and the nanofiller and the significance of nanofillers in improving nanocomposite properties. When combined with other characterization methods, UV−vis spectroscopy is an invaluable tool for evaluating the desirable optical characteristics of nanofillers in a polymer matrix. By carefully selecting the kind and content of nanofiller in a polymer matrix, additional fine-tuning of the required optical qualities may be achieved based on the examination of the polymer nanocomposite's absorption characteristics.[36,75]

Wu and co-workers[63] employed UV characterization to understand the interaction of organ-like Ti$_3$C$_2$ with PPy nanoparticles (Figure 6(d)). The following three points summarize the synergistic impact of organ-like Ti$_3$C$_2$ and PPy nanoparticles: First, the use of a synergistic effect between distinct electrode materials and diverse energy storage techniques to achieve high specific capacitance and outstanding cycle stability by combining PPy with pseudocapacitance behavior and Ti$_3$C$_2$ with an electric double-layer capacitor mechanism. Moreover, the intercalation of homogeneous PPy nanoparticles increases the interlayer spacing of Ti$_3$C$_2$, allowing more paths for electrolyte ion diffusion and charge transfer, resulting in the lowest charge transfer resistance and more active sites. Finally, the organ-like Ti$_3$C$_2$ is an excellent conducting substrate that efficiently inhibits PPy stacking and improves structural stability; therefore, it is helpful.[63]

Recently, Xian-Ying and colleagues[53] used the UV−Vis approach to analyze the adsorption and desorption capabilities of the MXene/PPy nanocomposite to remove organic pollutants such as methylene blue (MB) from the wastewater. The adsorption capacity of the MXene/PPy nanocomposite substantially increases to 345.1 mg/g when measured within the wavelength range of 200−800 nm, with MB at an absorption wavelength of 664.5 nm removal ratio reaching 89%. Their results reveal that adding PPy particles to MXene nanosheets improves the adsorption performance of the MXene/PPy composite particles. In other words, PPy and MXene appear to work together to eliminate MB. The considerably improved adsorption ability may be due to the increased exfoliation degree of MXene nanosheets and the better dispersion of MXene and PPy.[53]

3.5. XPS. The essential use of XPS in nanocomposites based on MXene/PPy permits the rapid generation of the chemical composition of MXene, pure PPy, and the MXene/PPy composite to determine the elemental composition, valence state, and effective interaction between an individual component of the composite. The goal of the XPS research on the MXene/ PPy surface has been to investigate the binding energy of photoelectrons released when MXene, pure PPy, and the MXene/PPy nanocomposite are exposed to X-rays. The existence of C, N, O, and Ti elemental components in MXene/PPy was shown by XPS.[47,61] While in sample Ti$_3$C$_2$, XPS signals from elements C, Ti, O, and F were observed.[63] For pure Ti$_3$C$_2$T$_x$, the Ti 2p core level spectra could be deconvoluted into four Gaussian peaks. The emergence of Ti−X and Ti−O
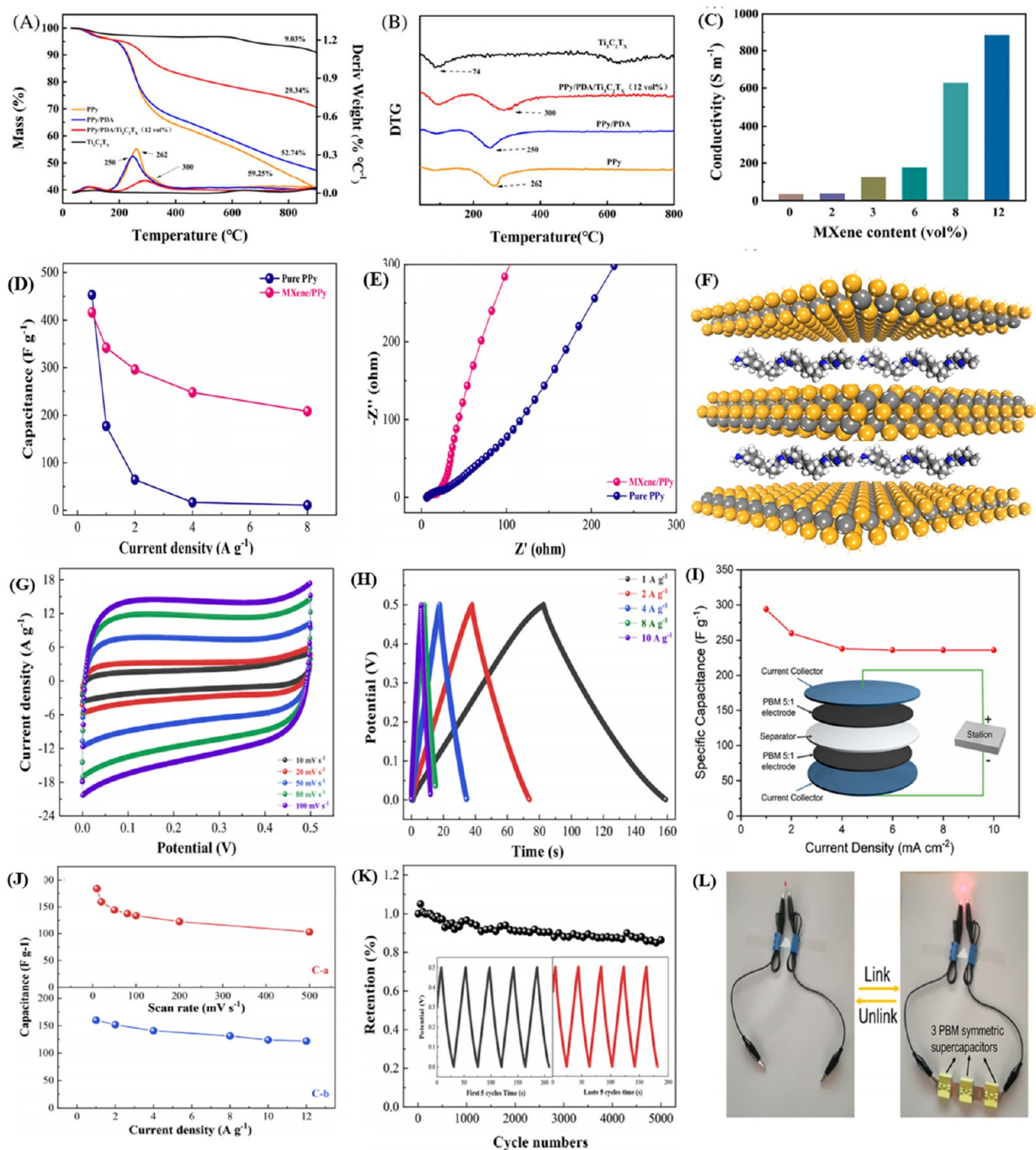
Figure 7. (a) TGA and (b) DTG of PPy, MXene, and PPy-based composites. (c) For varying $Ti_3C_2T_x$ loadings, the conductivity of PPy/PDA/$Ti_3C_2T_x$. Reprinted with permission from ref 78. Copyright 2022, John Wiley & Sons, Inc. (d) At varying current densities, the rate performance of a pure PPy electrode and an MXene/PPy composite film electrode. Reprinted with permission from ref 32. Copyright 2019, Elsevier Science Ltd. (e) MXene/PPy and pure PPy electrode EIS. Reprinted with permission from ref 32. Copyright 2019, Elsevier Science Ltd. (f) Demonstration of PPy chains intercalated within MXene for expanded interlayer spacing. The MXene/PPy symmetric supercapacitor device's electrochemical performance. (g) Curves of the CV at various scan rates and (h) curves of the GCD at various current densities. Reprinted with permission from ref 32. Copyright 2019, Elsevier Science Ltd. (i) Resultant gravimetric capacitance as a function of current density. Reprinted with permission from ref 70. Copyright 2021, Springer Nature. (j) Capacitance of the symmetric MXene/PPy supercapacitor device at varied scan rates and current densities. (k) At a current density of 5 A g^{-1}, the device's cycle stability was tested, and the GCD curves of the first and final 5 cycles were shown in the inset. Reprinted with permission from ref 32. Copyright 2019, Elsevier Science Ltd. (l) A red LED light is illuminated by three PBM symmetric supercapacitors connected in sequence. Reprinted with permission from ref 70. Copyright 2021, Springer Nature.

chemical bonds is attributed to the Ti 2p$_{3/2}$ peak at 455.0 eV and the Ti 2p$_{1/2}$ peak at 461.3 eV.[32] Similarly, the Ti 2p core level spectrum for Ti_3C_2/PPy may be deconvoluted into four peaks. The Ti−C 2p and Ti−O 2p peaks have different binding energies located at 455.16 and 458.93 eV and 458.79 and 464.51 eV, respectively.[34] Moreover, from the slew of XPS analyses reported on MXene/PPy nanocomposites, the deconvolution of the C 1s core level was reported to produce distinctive Gaussian

peaks of C—C at 284.6 eV, O—C═O at 288.3 eV, C—Ti at 284.3 eV, and disordered C at 289.5 eV, and the C—N is at 285.5 eV for pure PPy and MXene/PPy nanocomposites.[32,61,63] The formation of the carbonyl carbons (O—C═O) from the C 1s core spectrum is demonstrated to exhibit high binding energy, which is facilitated by the invasion of water during the electrochemical polymerization process.[34,57] Besides, the significance of this bond arises from the interaction of PPy with MXene, which depicts the formation of strong hydrogen bonding formed by the interaction of N—H moiety functional groups of MXene with pyrrole rings.[65] In addition, carbon atoms linked with sulfur atoms on the dopant exhibited weak binding energy at 283.4 eV.[57] The area of the peak is commonly used to calculate PPy's doping level. Zhu et al.[57] reported the CS peak area percentage for pure PPy to be 5.18%, whereas the CS peak area percentage for the l-Ti_3C_2/PPy film is 12.79%. In addition, on the higher-binding-energy side, the C 1s spectra of the l-Ti_3C_2/PPy film are more asymmetric; this is due to a broader peak at 286.4 eV, which is caused by disordered carbons. The peak area percentage of disordered carbon in the PPy/l-Ti_3C_2 film rose from 4.07% to 5.71%, perhaps due to interactions between PPy and l-Ti_3C_2.[57] Aside from the C 1s core spectrum, three peaks can be seen in the high-resolution N 1s spectra of pure PPy and Ti_3C_2/PPy: 399.4, 400.1, and 401.5 eV. The benzenoid amine (—NH—), protonation benzenoid amine (—N^+H—), and protonation quinonoid imine (═N^+—) are all assigned to these peaks, respectively.[32,34,70] The XPS, Ti 2p, C 1s, and N 1s core spectra of the MXene/PPy nanocomposite are shown in Figure 6(e and h). The MXene/PPy composite has a polaron (—N^+/N) ratio of 0.29, which is larger than pure PPy with a ratio of 0.21, indicating that the negatively charged MXene might act as a counteranion to balance the positively charged (Py^+).[32] The polaron ratio is the area ratio between the polaron peak (—N^+H— and —N^+═) and the total nitrogen peak (—NH—, —N^+H—, and —N^+═), which provides an insight into the magnitude of the ion participating in the electrochemical reaction.[70] The exposure of the MXene/PPy composite to elevated temperature can also lead to significant chemical changes. Lei et al.[61] investigated the difference in the chemical composition of MXene/PPy at different temperatures. The pyrrolic and positively charged (N^+) nitrogen peaks in the high-resolution N 1s spectra of MXene/PPy were deconvoluted into two peaks at 399.8 and 401.9 eV, respectively. It is worth noting that the N 1s spectrum of the MXene/PPy pulverized at 800 K showed the presence of pyridinic, pyrrolic, graphitic nitrogen, and oxidized N as a result of the carbonization at high temperature. These N groups contributed 17.62%, 11.19%, 66.33%, and 4.86% of the total N content of the MXene/PPy at 800, respectively. Besides, the graphitic nitrogen concentration of MXene/PPy at 800 K material was the highest.[61]

4. PROPERTIES OF MXENE/PPY NANOCOMPOSITES

4.1. Thermal Properties. The ability of polymer nanocomposites to withstand high temperatures is critical for their use in sophisticated technologies. The removal of dopants from the polymer causes a reduction of electrical conductivity at high temperatures.[77] Thermal conductivity, thermal stability, and thermal expansion characteristics are examples of material features that change with temperature.[25] Differential scanning calorimetry (DSC), thermogravimetry analysis/derivative thermogravimetry (TGA/DTG), and other thermal analysis techniques are used to investigate them. The temperature transition behavior of MXene/PPy nanocomposites may be

determined effectively using DSC. Besides, the thermal stability, commencement of material breakdown, and quantity of MXene in the polymer matrix may all be determined via TGA/DTG.[73]

Under an inert atmosphere, Wu and colleagues[63] evaluated the thermal stability of Ti_3C_2, PPy, and Ti_3C_2/PPy from ambient temperature to 800 °C. The resultant Ti_3C_2 TGA curve shows three different phases of mass loss at an 11.75% rate. Before reaching 100 °C, a gradual weight loss corresponds to the elimination of physically adsorbed water that has remained on the Ti_3C_2 surface. Second, the weight loss from 200 to 400 °C is primarily due to eliminating chemically absorbed water, which is OH groups attached to the Ti_3C_2 surface. Finally, the weight loss at 500−800 °C results from the carbonization of Ti_3C_2 and the high-temperature removal of connected F functional groups on the surface. Meanwhile, in the pure PPy TG curve, there are two separate phases of weight loss. When the temperature is less than 100 °C, the weight loss is mostly due to the evaporation of the remaining water on the surface of PPy, which is similar to Ti_3C_2. The PPy chain begins thermal disintegration at 200 °C, and at 800 °C, the rate of weight loss reaches 57.90%. However, the intercalation of PPy within Ti_3C_2 alleviated the thermal weight loss rate of the nanocomposite to about 8.09%.[63] This shows the stabilizing effect of the combinatory synergy of PPy with MXene. Similarly, Lei and co-workers[61] reported the excellent thermal resistance of the MXene/PPy nanocomposite. However, they attributed the weight loss after 120 °C to the removal of doped anions and decomposition of the PPy matrix.[61]

Datong and coscientists[78] introduced polydopamine (PDA) to stabilize further the thermal degradation associated with PPy, although the TGA curve of PPy/PDA was comparable to that of PPy, with a 52.74% weight loss at 900 °C. However, following compounding with $Ti_3C_2T_x$, PPy/PDA increased the initial step of deterioration from 200 to 243 °C, with a considerable upward shift in the thermal curve. The thermal stability of the PPy/PDA/$Ti_3C_2T_x$ composite was greatly increased when compared to PPy and PPy/PDA composites, and it is attributed to $Ti_3C_2T_x$ and PPy/PDA forming a stable multilayer structure (Figures 7(a) and (b)).[78]

In general, inorganic nanoparticles in the polymer matrix increase the thermal stability by acting as a superior insulator and mass transport barrier to the volatile compounds released during the breakdown.[79] Meanwhile, the electron mobilities and thermal conductivities of MXenes have been observed to be exceptional. For example, the thermal conductivity of Sc_2CF_2 was calculated to be 472 $Wm^{-1} K^{-1}$ for a flake length of 5 m. MXenes are a great reinforcing nanomaterial for polymer-based electronic devices due to this feature.[80]

4.2. Electrical Properties. The electrical conductivity of MXene has been demonstrated to be outstanding, with a value as high as 9880 S/cm.[25,81] Therefore, the inclusion of MXene in PPy was shown to significantly increase the electrical conductivity by facilitating electron transport within the PPy matrix. Song and a co-worker[70] investigated the effect of $Ti_3C_2T_x$ on the electrical conductivity of PPy@BC. The conductivity of pristine PPy@BC was 136 S m^{-1}; however, when $Ti_3C_2T_x$ was incorporated into PPy@BC to a mass ratio of 1:5, a significant increase up to 14,245 S m^{-1} was reported. This significant improvement was attributed to the conductive channel formed by the close contact of uniformly dispersed $Ti_3C_2T_x$ nanoflakes within the PPy@BC matrix. The hydrogen-bonding interactions between the N—H and O—H groups on PPy@BC and the oxygen-containing groups on the surface of $Ti_3C_2T_x$ are ascribed to the intercalation of PPy@BC nanofibers

into $Ti_3C_2T_x$ nanoflakes which promote close contact and prevent restacking.[70] Recently, Datong et al.[78] investigated the conductivity of PPy/polydopamine (PDA)/$Ti_3C_2T_x$ composites which were fabricated through facile polymerization and mixing methods for electromagnetic interference shielding (EMI) applications. The electrical conductivity of the resulting nanocomposite was significantly raised from 34.6 to 884.1 S·m^{-1} by changing the $Ti_3C_2T_x$ content from 0 to 12 vol % (Figure 7(c)).[78]

4.3. Electrochemical Performance. Electrochemistry is an effective technique for studying electron transport processes. The passage of electrons is connected to chemical changes in electrochemical energy storage.[82] Scientists use a variety of techniques to assess the electrochemical performance of samples. These include cyclic voltammetry (CV), a galvanostatic charge−discharge test (GCD), and electrochemical impedance spectroscopy (EIS). CV is a potent and widely used electrochemical method for studying molecular species reduction and oxidation processes. It is also useful for studying chemical processes that are triggered by electron transfer, such as catalysis.[82] The area under CV is a standard metric for determining an electrode's qualitative capacitance.[47,65]

Besides, GCD tests (also known as constant current charging/discharging) are frequently used to evaluate energy storage systems and materials, such as those used in electrochemical capacitors (ECs). GCD is the process of charging and discharging a material/system within a predetermined potential limit using continuous positive and negative currents; this process is frequently repeated for several cycles. GCD profiles are used to assess capacitive response quality, detect the existence of irreversible Faradaic processes, and calculate various essential EC figures of merit, including capacitance, capacity, energy, and power.[83] Meanwhile, ion diffusion mechanisms, charge transfer kinetics, and internal resistance can be studied using EIS.[84]

You et al.[76] studied the electrochemical characteristics of the MXene/PPy nanocomposite. In 0.05 M PBS, the electrochemical conductivity of the bare glassy carbon electrode (GCE), pure PPy-modified electrodes, and MXene/PPy-modified electrodes was determined using the cyclic voltammetry (CV) test. The MXene/PPy-modified electrode revealed two pairs of redox peaks, namely, the oxidation peaks at 0.21 and 0.48 V as well as the reduction peaks at 0.17 and 0.31 V, which correspond to the electrocatalytic processes of MXene and PPy, respectively, as compared to the pure PPy-modified electrode.[76]

Meanwhile, the performance of the MXene/PPy composite and pure PPy film electrodes was examined at various current densities by Jian et al.[36] (Figure 7(d)). The 3D nanostructure of the MXene/PPy electrode was reported to be responsible for its improved rate capacity for capacitance retention of 50% when the current density is increased by 40 times (from 0.5 Ag to 8g). The ion transport and charge-transfer resistance (R_{ct}) of the MXene/PPy composite and pure PPy electrodes are shown in Nyquist plots (Figure 7(e)). The pure PPy film and MXene/PPy composite electrode exhibit a significant R_{ct} of ∼24 Ω and ∼12 Ω, respectively.[32] High capacitance and ultrastable bending and cycling performance are achievable when PPy is intercalated into l-Ti_3C_2 particles (Figure 7(f)). As a result, the capacitance reported rises as high as 30%, and after 20k charging/discharging cycles, the capacitance remained at 100%.[57] When MXene/Ppy composite-film-coated ITO glasses were used to develop an electrochemical supercapacitor, during the charging/discharging process, the device had low resistance and a high degree of

reversibility. The device retained around 86.4% of its charge and had excellent cycle performance (Figure 7(g) and (h)).[32]

A decrease in capacitance is typical of pseudocapacitive electrodes at increasing scan rates.[43] Thus, when the gravimetric capacitance of the PPy@bacterial cellulose/MXene nanocomposite (PBM) symmetric supercapacitor was calculated from the discharge curve of GCD (Figure 7(i)) at a current density of 1 mA·cm^{-2}, it was 294 F·g^{-1}. By increasing the PPy content, PBM 5:1 has the maximum capacitance of 550 F·g^{-1} (879 mF·cm^{-2}) as the area of the curve steadily grows. When the charging and discharging current gradually increases, the PBM electrode exhibits excellent capacitance retention. In addition, an energy density of up to 33.1 Wh·kg^{-1} was obtained with the same capacitance.[70] However, Jian et al.[32] showed that as the scan rates and current densities increase the capacitance of the MXene/PPy symmetric supercapacitor reduces (Figure 7((j) and (k)).[32] Figure 7(l) demonstrates the illumination of a red LED light by three PBM symmetric supercapacitors connected in sequence after charging to 3 V.[70]

5. ENERGY STORAGE APPLICATIONS

5.1. Supercapacitors. Owing to their unique features, supercapacitors (SCs) are considered one of the most promising energy-storage technologies.[85] The three types of supercapacitors are electrochemical double-layer capacitors, pseudocapacitors, and hybrid capacitors. The pseudocapacitors are supercapacitors that attract the attention of polymer scientists and engineers. This supercapacitor chemically stores charge at the electrode surface via a Faradaic redox process. During the charging and discharging operation, the electrode material stores charges. Among the potential electrode materials suitable for pseudocapacitor devices, conductive polymers have emerged as one of the most promising electrode materials. This is primarily due to their low cost, high capacitance, excellent electrical conductivity, fast charge and discharge, and environmentally benign characteristics.[86] Prime examples of CPs used for pseudocapacitors include polyaniline (PANI), polyfuran (PF), PPy, poly(3,4-ethylene dioxythiophene) (PEDOT), polythiophene (PTH), and poly(para-phenylene) (PPP).[87]

Because of its low cost, high electrical conductivity, and intriguing redox characteristics, PPy has been investigated as a viable electrode material for high-performance supercapacitors.[88] When pure PPy is employed as electrode material in energy storage devices, however, there is a major deterioration concern.[47] Based on this premise, the use of PPy for energy storage is generally found in a composite state with conductive pseudocapacitive inorganic compounds.[11,52,89−101]

An interesting inorganic filler that has garnered immense attention recently from researchers for improving the energy storage integrity of PPy is the MXene. MXenes have already proven to be viable candidates for electrodes in lithium (Li)-ion batteries and supercapacitors, with volumetric capacitances that outperform the majority of previously reported materials.[11,102] In a three-electrode arrangement, delaminated $Ti_3C_2T_x$, notably, has exhibited exceptional capacitance values up to 1500 F cm^3 (380 F g^{-1}) in aqueous electrolytes.[89] MXene, an atomically thick titanium carbide, is a universal pseudocapacitive anode material for a variety of CP-containing electrodes.[67,103,104] As such, PPy may be intercalated between the layers of $Ti_3C_2T_x$ nanosheets, increasing the distance between them and therefore increasing the rate of charge transfer in energy storage devices. Conductive routes also aid the charge's movement via the percolation channels. MXenes are distin-

guished by the structure that makes them particularly appealing for electrochemical energy storage.[105] This is largely due to the presence of the transition metal carbide core that allows for metallic conductivity of up to 10,000 S cm^{-1} for rapid electron mobility, the presence of redox-active surface owing to the presence of transition metal oxide, and the availability of termination groups such as −F, −OH, and −O.[11]

By intercalating PPy into layered Ti_3C_2, Zhu et al.[90] created conductive polymer-based freestanding flexible electrodes with considerably better electrochemical performances. Figure 8(a)
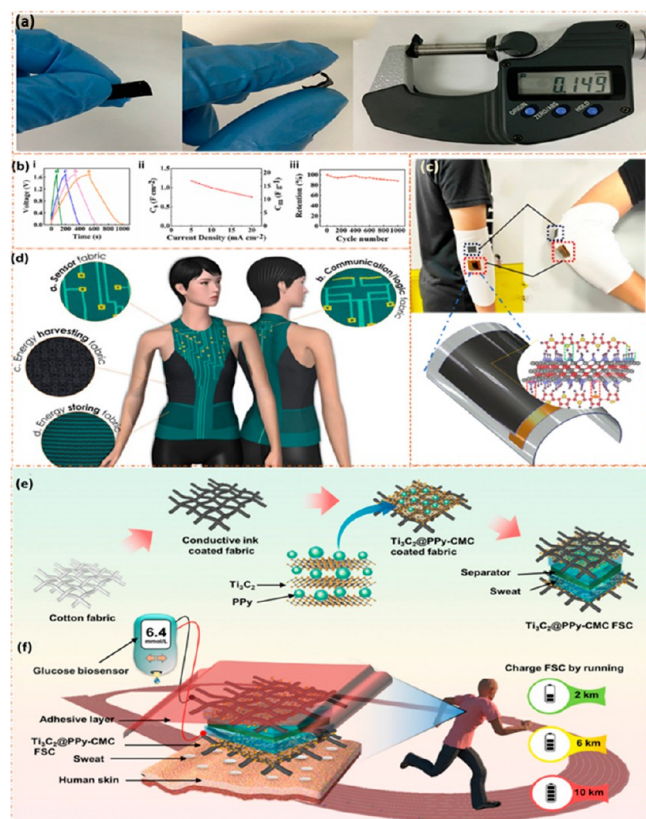

Figure 8. (a) Symmetric solid-state flexible as-prepared supercapacitor based on the l-Ti_3C_2/PPy film and the measured thickness. Reprinted with permission from ref 57. Copyright, 2016, Wiley-VCH Verlag GmbH & Co. KGaA, Weinheim. (b) Electrochemical performance of MXene/PPy-based asymmetric SC from GCD data. Reprinted with permission from ref 72. Copyright 2022, Elsevier Science Ltd. (c) Illustrative schematic representation of wearable FSC made from MXene/PPy. Reprinted with permission from refs 53 and 117. Copyright 2022, Elsevier Science Ltd. and Copyright 2021, John Wiley & Sons, Inc., respectively. (d) Ti_3C_2/PPy-based FSC in wearable electronic textiles for energy storage, harvesting, and sensor applications. Reprinted with permission from ref 118. Copyright 2015, John Wiley & Sons, Inc. Ti_3C_2@PPy-CMC FSC patch that may be applied to the skin: (e) Ti_3C_2@PPy-CMC FSC fabrication method and (f) schematic representation of the Ti_3C_2@PPy-CMC FSC patch, which is powered by human perspiration during exercise. Reprinted with permission from ref 116. Copyright 2022, Elsevier Science Ltd.

illustrates $Ti_3C_2T_x$/PPy-based freestanding flexible electrodes. The capacitance of the resulting nanocomposites was as high as 203 mF cm^2 (406 F cm^3). Furthermore, even after 20,000 charging/discharging cycles, about 100% capacitance retention is obtained. According to the findings, the intercalation of PPy prevents the unavoidable restacking of MXene sheets, which impedes the diffusion and mass transfer processes and

electrolyte infiltration.[90] Furthermore, strong linkages produced between the PPy backbones and surfaces of l-Ti_3C_2 increase the structural stability of PPy backbones while simultaneously ensuring high conductivity and providing precise routes for charge-carrier transport. The freestanding l-Ti_3C_2/PPy film is also utilized to build an ultrathin all-solid-state supercapacitor with an exceptional capacitance (35 mF cm^{-2}) and steady performance through 10,000 charging/discharging cycles.[57] The $Ti_3C_2T_x$/PPy composite fabricated using the oxidant-free polymerization process resulted in an oriented PPy confined between the conductive $Ti_3C_2T_x$ monolayers in a self-assembled layered architecture and has a volumetric capacitance of about 1000 F cm^{-3} with high capacitance retention of 92% after 25,000 cycles.[43]

It has been reported that structural modification and nanoarchitecture engineering significantly improve the electrochemical capacitance of MXene/PPy. As a result, several scientists and engineers have created MXene/PPy with diverse morphologies and topologies, such as a 2D and 3D $Ti_3C_2T_x$/PPy nanowire network,[65,106] organ-like $Ti_3C_2T_x$/PPy,[63] carambola-like MXene/PPy,[32] ionic-liquid-based MXene/PPy,[107] and MXene/(BC)@PPy.[70] The carambola-like MXene/PPy composite enabled electron transport and ionic diffusion in a three-dimensional (3D) network. The organ-like Ti_3C_2 framework restricts PPy growth, lowers $Ti_3C_2T_x$ stacking, and increases the structural stability of the Ti_3C_2/PPy nanocomposite.[63] Microemulsions based on ILs that spontaneously adsorb onto $Ti_3C_2T_x$/PPy nanosheets are envisioned as another liquid "spacer", enabling rapid ion diffusion kinetics and no electrolyte imbibition stages.[107] Meanwhile, BC effectively adjusts the morphology of PPy nanoparticles to prevent dense packing.

Besides, the voltage profiles of various MXenes have also been shown to demonstrate erratic results, implying that distinct MXenes are suitable for anode or cathode applications as well as for symmetric and asymmetric supercapacitors.[108] Symmetrical[32,33,62] and asymmetrical[72,103,109] electrode designs involving PPy and MXene result in supercapacitors with differential and intriguing features that exhibit a high volumetric and specific capacitance but also an exceptional cycle life, resulting in enhanced long-term stability.[87] For instance, in asymmetric SC construction, the working voltage window of $Ti_3C_2T_x$-based microsupercapacitors (MSCs) is relatively limited (0.6 V), which limits its practical applicability. However, the fabrication of the $Ti_3C_2T_x$/PPy/MnO_2 nanocomposite exhibited an extended working voltage to about 1.2 V. Moreover, its maximal areal capacitance and areal energy density, respectively, were as high as 61.5 mF cm^2 at 2 mV s^{-1} and 6.73 Wh cm^2 at 204 W cm^2 with over 80.7% capacitance retention after 5000 cycles at 1.72 mA cm^2.[110] On the other hand, manufacturing asymmetric supercapacitors with significantly different anodes is another technique to widen the voltage window of MXene/PPy nanocomposites to obtain high energy density.[89] Thus, owing to the low active mass loading (AML) in symmetric SC and the limitation in the operating voltage windows of 0.5^{-1} V in acidic electrolytes, Liang and co-workers[72] explored the electrochemical performance of an asymmetric SC. In the presence of an anionic dopant (multiwalled carbon nanotubes (MCNTs)), the asymmetric SC device operating in a neutral 0.5 M Na_2SO_4 electrolyte with a voltage window of 1.7 V had a high capacitance of 2.11 F cm^2 from CV data and 2.49 F cm^2 from GCD data (Figure 8(b)).[72]

Table 2. Energy Storage Performance of MXene/PPy Nanocomposite-Based Supercapacitors[a]

Species	Electrolyte	Capacitance (rate)	Energy and power densities	Cycling stability	Ref
Ti_3C_2	6 M KOH	47 F g^{-1} at 0.5 A g^{-1}	-	80% (1000)	34
	1 M H_2SO_4	132 F g^{-1} at 2 mV s^{-1}	-	-	34
	1 M Na_2SO_4	133.91 F g^{-1} at 2 mV s^{-1}	-	-	63
PPy	1 M H_2SO_4	374 F g^{-1} at 2 mV s^{-1}	-	-	34
	1 M Na_2SO_4	155.69 F g^{-1} at 2 mV s^{-1}	-	-	63
PPy	1 M H_2SO_4	128 F g^{-1} at 1 A g^{-1}	-	50% (1000)	47
PPy NW		304 F g^{-1}	-	-	106
$Ti_3C_2T_x$/PPy	1 M H_2SO_4	266 F g^{-1} at 1 A g^{-1}	-	-	47
$Ti_3C_2T_x$/PPy	0.5 M Na_2SO_4	2.11 cm^{-2}	-	-	72
NA-$Ti_3C_2T_x$/PPy	1 M H_2SO_4	318 F g^{-1} at 1 A g^{-1}	-	-	47
NA-CTAB-$Ti_3C_2T_x$/PPy	1 M H_2SO_4	437 F g^{-1} at 1 A g^{-1}	-	76% (1000)	47
Ti_3C_2/PPy-2	1 M Na_2SO_4	184.36 F g^{-1} at 2 mV s^{-1}	21.61 Wh kg^{-1} (499.94 W kg^{-1})	83.33% (4000) at 1 A g^{-1}	63
		458 F g^{-1} at 2 mV s^{-1}		73.68% (4000) at 1 A g^{-1}	
Ti_3C_2/PPy	-	1000 F cm^{-3}	-	92% (25 000)	43
2D $Ti_3C_2T_x$/PPy NW	-	416 F g^{-1} at 0.5 A g^{-1}	-	86.4% (5000) at 5 A g^{-1}	32
		184 F g^{-1} at 10 mV s^{-1}			
2D $Ti_3C_2T_x$/PPy NW	-	374 F g^{-1} at 10 mV s^{-1}	-	91.6% (2000)	106
3D $Ti_3C_2T_x$/PPy NW	-	610 F g^{-1}	-	100% (14,000) at 4 A g^{-1}	65
l-Ti_3C_2/PPy	PVA-H_2SO_4	150 (300) to 203 mF cm^{-2} (406 F cm^{-3})	-	100% (20,000)	57
l-Ti_3C_2/PPy	-	35 mF cm^{-2}		10000	57
$Ti_3C_2T_x$/PPy	-	343.20 F g^{-1}	-	-	33
$Ti_3C_2T_x$/PPy	2 M H_2SO_4	109.4 mF cm^{-2} at 1.05 mA cm^{-2}	3.398 μWh/cm^2 (0.0845 mW/cm^2)	96% (10,000)	69
	PVA-H_2SO_4	86.7 mF cm^{-2} at 1.05 mA cm^{-2}	2.028 μWh/cm^2 (0.338 mW/cm^2)		
PPy/Ti_3C_2–S1	1 M H_2SO_4	380 F g^{-1} at 2 mV s^{-1}	-	-	34
PPy/Ti_3C_2–S2	1 M H_2SO_4	458 F g^{-1} at 2 mV s^{-1}	-	-	34
PPy/Ti_3C_2–S3	1 M H_2SO_4	346 F g^{-1} at 2 mV s^{-1}	-	-	34
MXene/PPy/PMFF	1 M H_2SO_4	1295 mF cm^{-2} at 1 mA cm^{-2}	-	94.8% (30,000)	62
	-	1062.5 mF cm^{-2} at 50 mA cm^{-2}	-	-	62
MXene/PPy/PMFF	1 M H_2SO_4	439 F g^{-1} at 1 mA cm^{-2}	-	-	62
	-	360 F g^{-1} at 50 mA cm^{-2}	-	-	62
MXene/PPy/PMFF	PVA/Na_2SO_4 gel	458 mF cm^{-2} at 1 mA cm^{-2}	29.2 μW h cm^{-2} at 25 mW cm^{-2}	93.7% (30,000)	62
			40.7 μW h cm^{-2} at 0.5 mW cm^{-2}		
	-	328 mF cm^{-2} at 50 mA cm^{-2}	-	-	62
$Ti_3C_2T_x$//PPy/MnO_2	PVA/H_2SO_4	61.5 mF cm^{-2} at 2 mV s^{-1}	-	80.7% (5000)	110
IL-$Ti_3C_2T_x$//PPy	-	-	31.2 Wh kg^{-1} (at 1030.4 W kg^{-1})	91% (2000)	107
PPy@BC/$Ti_3C_2T_x$	-	550 F g^{-1}	33.1 W h kg^{-1} (243 W kg^{-1})	83.5% (10,000)	70
		879 mF cm^{-2}			
		294 F g^{-1} at 1 mA cm^{-2}			
(MXene/PPy)@Cotton	-	455.9 mF cm^{-2} at 0.9 mA cm^{-2}	-	-	115
	-	506.6 F g^{-1} at 1 A g^{-1}	-	-	115

[a]NA: 1,5-naphthalene disulfonic acid. CTAB: cetyltrimethylammonium bromide.

The introduction of mechanical flexibility into the design of electrodes for energy storage has led to the development of a flexible supercapacitor (FSC).[84,111−114] Therefore, owing to the rapid charging rates, simple fabrication method, and outstanding cycle stability, the flexible supercapacitor (FSC) has emerged as a feasible option in wearable electronics with better electrochemical performance. As a result, Yan and his colleague[33] electrochemically deposited PPy on the surface of MXene textiles, resulting in high specific capacitance (343.20 F g^{-1}). Furthermore, the symmetrical solid-state SCs based on MXene−PPy fabric devices exhibit excellent electrochemical performance and flexibility.[33] MXene flakes are used as an ultrafast electron transport layer on fiber fabric for high-performance textile electrodes. For instance, cotton fiber electrodes with high specific capacitance increased by in situ hybrid polymerization of PPy and MXene (Figure 8(c)). At a current density of 1 A g^{-1}, the mass and areal capacitance of the constructed (MXene/PPy)@Cotton electrode are, respectively, 506.6 F g^{-1} and 455.9 mF cm^{-2} at a scan rate of 0.9 mA cm^{-2}. Figure 8(d) illustrates the application of Ti_3C_2/PPy-based FSCs in wearable electronic textiles.[115] Jayraj and colleagues[116] created biocompatible Ti_3C_2 nanosheets and the polypyrrole-carboxymethylcellulose nanosphere Ti_3C_2@PPy-CMC composite for a skin-attachable FSC that uses biofluid (sweat) as an electrolyte (Table 2, Figure 8((e) and (f)).[116] Similarly, the MXene/PPy/PEI-modified fiber fabric (PMFF) textile electrode created by Li and colleagues[62] has high capacitance, outstanding rate capacity, and extraordinary cycle stability. Even at high discharge rates, the areal capacitance of MXene/PPy/PMFF showed no appreciable reduction. At 1 mA cm^{-2}, it offers 1295 mF cm^{-2} of areal capacitance, with an ultrahigh value of 1062.5 mF cm^{-2} maintained even at a high discharge rate of 50 mA cm^{-2}.[62]
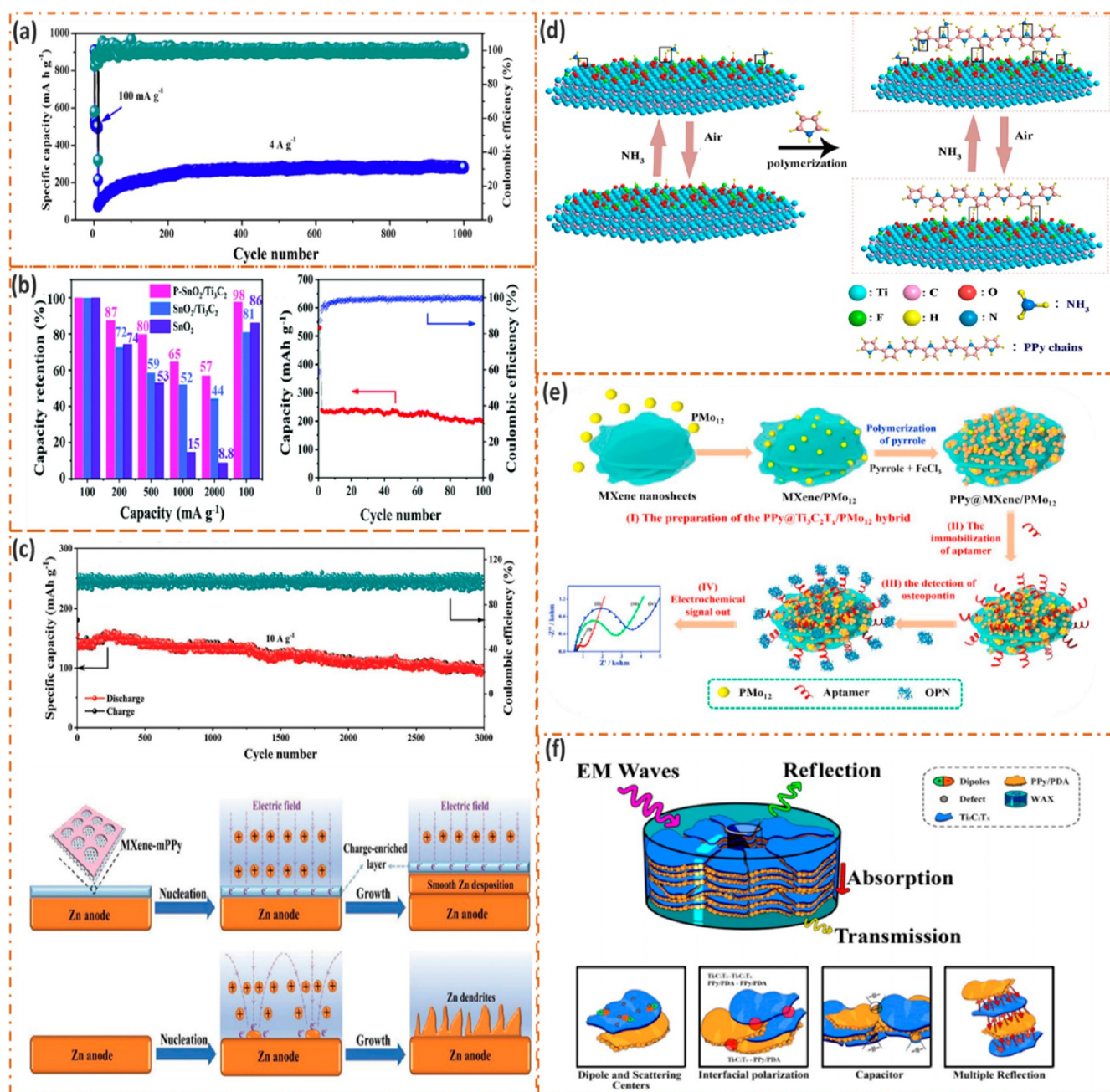
Figure 9. Cycling performances of (a) $TiO_2@NC/Fe_7S_8$ at 4 A g^{-1}. Reprinted with permission from ref 60. Copyright 2020, Elsevier Science Ltd. (b) P-SnO_2/Ti_3C_2 electrode at a large current density of 2000 mA g^{-1}. Reprinted with permission from ref 66. Copyright 2021, Royal Society of Chemistry. (c) MnO_2/MXene-mPPy/Zn cell at 1 A g^{-1}. Reprinted with permission from ref 130. Copyright 2022, John Wiley & Sons, Inc. Schematic illustration of the (d) MXene/PPy nanocomposite as a sensor for NH_3 gas. Reprinted with permission from ref 137. Copyright 2022, Springer Nature Switzerland, AG. (e) The development of PPy@$Ti_3C_2T_x$/PMo_{12} for the detection of osteopontin. Reprinted with permission from ref 35. Copyright 2019 Elsevier Science Ltd. (f) PPy/PDA/$Ti_3C_2T_x$ composites as EMI shielding. Reprinted with permission from ref 78. Copyright 2022, John Wiley & Sons, Inc.

5.2. Battery. Rechargeable lithium-ion batteries (LIBs) have piqued attention due to their lack of memory effect and higher energy densities and have been widely employed in portable gadgets and electric vehicles for decades. Electrode materials, being the most significant component of LIBs, play a critical role in determining their performance. Because of their high theoretical capacity, high electric conductivity, and vast chemical and structural variation, 2D materials, particularly the developing MXenes, have a lot of potential for next-generation LIB electrodes.[11,108]

MXenes are well-known for their ability to act as pseudocapacitive materials, and they like to be employed in this manner.[119] MXene was originally studied as a LIB anode material by Naguib et al.[11] in 2011 and showed encouraging results.[108] As such, open structures, numerous surface groups, high electrical conductivity, and high ion/electron transfer efficiency in the MXene/PPy nanocomposite show considerable promise for developing next-generation high-performance rechargeable batteries.[11] For example, Mahajan and colleagues[120] developed polypyrrole-encapsulated polyoxomolybdate-decorated MXene as a functional 2D/3D nanohybrid for a

Li-ion battery that is both durable and high performing. Using a simple synthetic approach, they created polypyrrole-encapsulated polyoxomolybdate (PMo_{12})-decorated $Ti_3C_2T_x$ (PMo_{12}@$PPy/Ti_3C_2T_x$) and tested it as a lithium storage anode material. The PPy molecules surround the individual PMo_{12} anions and assist with effective intercalation between the layers of $Ti_3C_2T_x$ due to the electrostatic repulsion and self-assembly capabilities of PMo_{12} anions. As a result, the composite electrode has a large capacity of about 764 mAh g^{-1} at 0.1 A g^{-1}, extended cycling stability as high as 2000 cycles at 3 A g^{-1}, and outstanding rate performance. Because of the synergistic impact of PPy-encapsulated PMo_{12} and $Ti_3C_2T_x$, this unique 2D/3D design shows hybrid battery-capacitive behavior. Reversible redox processes of metal ions (Mo) contribute to the battery component, whereas PPy and $Ti_3C_2T_x$ contribute to the pseudocapacitive component. These findings show that MXene-based hybrid materials with the right engineering have a lot of potential in the field of energy storage.[120]

Zhang and his colleagues[60] investigated the energy storage features of a three-dimensional (3D) TiO_2@nitrogen-doped carbon/Fe_7S_8 composite made from PPy-encapsulated alkalized MXene as anode material for high-performance lithium-ion batteries. A straightforward hybrid technique was employed to create the 3D TiO_2@nitrogen-doped carbon (NC)/Fe_7S_8 composite, which involves in situ polymerization of a pyrrole monomer with alkalized $Ti_3C_2T_x$ and subsequent vulcanization at 700 °C. The TiO_2@NC/Fe_7S_8 exhibits a high reversible capacity of 516 mAh g^{-1} after 100 cycles at 0.1 A g^{-1}, outstanding rate capability of 337 mAh g^{-1} at 1 A g^{-1}, and strong extended cycling stability of 282 mAh g^{-1} after 1000 cycles at 4 A g^{-1} when used as an anode material for LIBs (Figure 9a).[60]

Besides, the effectiveness of the organic electro-active group (C=N) as a redox-active site has made PPy-based nanocomposites appealing for use in rechargeable aqueous batteries (RABs). As a result, Li and colleagues[121] investigated using MXene/PPy composites in flexible aqueous batteries. In an acidic aqueous electrolyte, the MXene@PPy composite has a large specific capacity of 124.9 mAh g^{-1} at 1.0 mA cm^{-2}, a high Coulombic efficiency of 100%, superior charge-transfer capability, excellent rate performance, and long-term cycling stability with high-capacity retention of 80.3% over 2500 cycles.[121]

LIBs are primarily utilized in portable electronic gadgets and large grid storage systems, but limited lithium supplies, growing costs, and safety concerns may restrict their use. On the other hand, sodium-ion batteries (SIBs) are seen as a possible alternative to LIBs due to their abundant supply, low cost, high-energy density like LIBs, and similar redox potential ($E_{Na/Na+}$ = 2.71% vs SHE, $E_{Li/Li+}$ = 3.04%). Unfortunately, the ionic radius of sodium (1.02) is greater than that of lithium (0.76), resulting in SIBs having a completely different electrochemical behavior than LIBs. For example, sodium ions cannot be intercalated into commercially available graphite anodes due to a lack of interlayer space. MXenes can tolerate ions of varied sizes because of their flexible interlayer space and excellent conductivity, indicating that they have considerable promise for high-performance SIB applications.[11,122−128] As such, by rationally designing and synthesizing TMO-based hybrid structures and accurately controlling the movement of ions and electrons, Ding and colleagues[66] overcame the barrier of creating transition metal oxides (TMOs) as anode materials for sodium-ion batteries (SIBs). These scientists used a simple in situ interfacial growth technique to create a new sandwich-

structured P-SnO_2/Ti_3C_2 composite, in which SnO_2 nanocrystals were modified with a 3 nm PPy layer tightly associated with $Ti_3C_2T_x$ MXene nanosheets through Sn−O−Ti chemical interactions. The conductive polymers PPy and $Ti_3C_2T_x$ serve as strong protective layers, easing volume expansion and providing rapid pathways for Na ions and electron transport, while uniformly dispersed SnO_2 nanocrystals enclosed in PPy and $Ti_3C_2T_x$ nanosheets provide plentiful active sites. The resultant P-SnO_2/Ti_3C_2 anode has good sodium storage qualities in terms of extended cycle life (325.6 mAh g^{-1} at 100 mA g^{-1} after 100 cycles) and rate performance due to the benefits of structure and composition (204.4 mAh g^{-1} at 1000 mA g^{-1}) (Figure 9(b)).[66]

Other metal ions with varying sizes and valences, such as zinc,[129] can be intercalated into 2D MXenes/PPy in addition to lithium and sodium ions. Although Zn metal anodes have certain inherent benefits for aqueous zinc ion batteries, their renowned dendrites limit their practical use. Thus, Zhang and colleagues[130] investigated a dendrite-free Zn metal anode using a charge-enriched approach based on MXene/PPy layers. The nanocomposite's charge enrichment ability is exceptionally high, up to 149 F g^{-1} and 5 mV s^{-1}, which is advantageous for accumulating charge levels. As a result, the team created a dendrite-free Zn anode with a cycle lifespan of up to 2500 h and better rate capability, which could also serve as an anode for aqueous zinc, having a long-term cycle life of 3000 cycles at 10 A g^{-1} (Figure 9(c)).[130]

5.3. Other Applications of Polypyrrole/MXene Nanocomposites.
5.3.1. Sensor, Electromagnetic Interference (EMI) Shielding, and Electrocatalysts.
Electrochemical sensors transform chemical reactions of target analytes on electrodes into electrical signals that cause conductivity, potential, or current changes.[131] The conducting polymer such as PPy is an excellent choice for electrochemical sensors due to its remarkable electrical characteristics, customizable chemical structures, and ease of production.[132−135] Besides, conductive inorganic nanofillers such as MXene have strong conductivity, have a low bandgap, are simple to functionalize, and have a lot of active sites, making it ideal for sensors with high sensitivity and selectivity.[25,136]

Therefore, by combining MXene with PPy, You and co-workers[76] developed a chemical sensor for duo identification of dopamine (DA) and uric acid (UA) amidst ascorbic acid (AA) interference. In the presence of a high concentration of AA, the MXene/PPy nanocomposite-modified electrode showed a low detection limit (DA: 0.37 μM, UA: 0.15 μM) as well as a wide linear range (DA: 12.5−125 μM, UA: 50−500 μM) and the selective determination of DA and UA. More crucially, the as-prepared sensor effectively performed simultaneous sensing for the coexistence of DA and UA.[76]

Moreover, the MXene/PPy nanocomposite was used as a sensor for NH_3 gas (Figure 9(d)). When the MXene/PPy nanocomposite is exposed to NH_3 gas, its resistance rises, which is typical of p-type semiconductors. The deprotonation/protonation mechanism generated by the adsorption/desorption of NH_3 on the surface of nanocomposites might explain the sensing response of MXene/PPy nanocomposites to NH_3. When the nanocomposites are submerged in NH_3, the ammonia molecule interacts with MXene/PPy. The nitrogen in ammonia loses an electron to the nitrogen in the main chain of the polymerization to form an ammonium ion, similar to deprotonation and resulting in a resistance change. When the sensor is withdrawn from the NH_3 environment and

reintroduced to the air, its resistance will be totally or partially restored.[137]

Similarly, as illustrated in Figure 9(c), Zhou and colleagues[35] investigated the feasibility, sensitivity, and reliability of the $Ti_3C_2T_x$ MXene and polyoxometalate nanohybrid embedded with PPy@ $Ti_3C_2T_x$/PMo_{12} for the detection of osteopontin. The nanocomposite not only exhibited a wide range of chemical functions, a high degree of crystallinity, and a homogeneous surface shape but also had good electrochemical activity. Due to these characteristics, the nanocomposite has exceptional stability, great biocompatibility, and a significant binding force toward OPN aptamer strands. Thus, compared to previously developed bicomponent aptasensors, the hybrid demonstrated improved electrochemical sensing. Accordingly, the aptasensor has a detection limit of 0.98 fg mL^{-1}, strong selectivity and stability, reasonable renewability, good repeatability, and application in human blood samples.[35]

Besides sensors, electrocatalysts and EMI shielding are among the uses for MXene/PPy-based nanocomposites. Due to their superior electrical conductivity, low weight, and outstanding EMI shielding performance, MXene/PPy nanocomposites have emerged as primary and potential wearable EMI shielding materials. The EM wave absorption characteristics of $Ti_3C_2T_x$/PPy hybrids were explored by Tong and colleagues.[138] It is reported that composites containing a fraction of $Ti_3C_2T_x$/PPy (0.25 wt %) in a paraffin matrix with a thickness of 3.2 mm have about 99.99% absorption capability with a minimum reflection loss of 49.2 dB. Meanwhile, with an absorber thickness of 2.0 mm, a maximum effective absorption bandwidth of 4.9 GHz was achieved. Furthermore, by altering the thickness from 1.5 to 5.0 mm, a 13.7 GHz (4.3−18.0 GHz) effective absorption bandwidth may be achieved. Additionally, when the mass fraction is 15 wt %, the largest effective absorption bandwidth of 5.7 GHz is achieved.

Recently, in the X- and Ku-bands (Figure 9(f)), Wu et al.[78] examined the electromagnetic interference shielding characteristics of PPy/PDA/$Ti_3C_2T_x$ composites by varying $Ti_3C_2T_x$. At a filler content of 12 vol %, the resultant PPy/PDA/$Ti_3C_2T_x$ composites showed a commensurate increase in the maximum EMI SE in the Ku-band from 4.30 to 21.82 dB. Although, in pure PPy, a little reflection of electromagnetic waves occurs due to the conductive characteristics of PPy.[139,140] However, compared to PPy, the PPy/PDA/$Ti_3C_2T_x$ composite plays a crucial role in electromagnetic radiation suppression. The continuous MXene layers with strong electrical conductivity alternatively layered with PPy and PDA explain the multilayer structures' significant improvement in EMI attenuation capabilities. Because the etched 2D MXene has a lot of vacancy-related defects, such as polarization centers and dipoles made up of functional groups and their dangling bonds, the remaining incident EW waves will be attenuated even more.[78,141]

The oxygen reduction reaction (ORR) is a critical electrochemical mechanism for converting the energy in fuel cells and metal-air batteries.[87,142] For energy conversion, MXene/PPy has shown good catalytic activity. Lei et al.[61] demonstrated the development of MXene/PPy nanocomposites that can function as an oxygen reduction reaction (ORR) catalyst. The resultant catalyst had 9.6% nitrogen that was evenly distributed. During the ORR, this catalyst's onset and half-wave potentials were 0.85 and 0.71 V, respectively. The high concentration of graphitic nitrogen, which was 80.6%, was credited with remarkable catalytic activity. Moreover, the catalyst performed better than a commercial Pt/C catalyst in terms of long-term stability during ORR.[61]

6. CONCLUSION AND OUTLOOK

This paper covers current advances in MXene/PPy architecture preparation, characterization, and characteristics, as well as their application in electrochemical energy storage and conversion. MXene/PPy can be made via oxidative and oxidant-free in situ polymerization, electrochemical polymerization, and solution mixing techniques. All these approaches have been examined, with chemical polymerization being the most extensively employed. Electrical characteristics and thermal stability are often improved when MXene is introduced. However, the electrochemical characteristics of MXene/PPy nanocomposites are often superior to those of pure PPy and provide synergistic pseudocapacitive behavior not found in pristine MXene. Consequently, MXene's interlayered stacking prevents PPy agglomeration around it, while PPy's intercalation prevents MXene's dense stacking, resulting in high ion/electron transfer efficiency in MXene/PPy. Apart from individual component properties, the degree of dispersion of MXene nanoparticles in the PPy matrix, as well as the shape of PPy nanoparticles in the nanocomposite system, nanoarchitecture, and interfacial interaction, all play important roles in enhancing or limiting the overall properties of the system. Despite the fact that significant study has been done on various aspects of MXene/PPy nanocomposites, this class of material is still in its infancy, and more research is needed to explore the wide range of MXenes available with PPy and better understand the complicated structure−property interactions. Customizing the MXene/PPy interfacial interaction leads to a better understanding of the relationships.

Furthermore, its storage capacity for LIB, SIB, and ZnB applications has proven promising, but further research is needed in this area as well as for metal-ion batteries in general. MXene/PPy has also demonstrated exceptional performance as a pseudocapacitive electrode material for supercapacitors. It is, however, recommended to explore a wide range of possible MXene/PPy nanocomposites for a variety of applications, such as metal-ion batteries, supercapacitors, EIS, electrochemical sensors, and general flexible and wearable electronics. Further investigation of these materials, including their stability across operating temperatures, electrode degradation, and safety, should be encouraged

Besides, chemical functionalization and nanoengineering can equally expand the functionality and processability of this class of materials. By exploring a wide range of potential dopants, it is possible to enhance the storage capability, along with the rate of performance and cyclic stability of MXene/PPy nanocomposites. Doping has been demonstrated to be a robust process for preventing 2D materials from agglomerating in dissolvable media by preserving their high specific surface area and large aspect ratio, improving wettability, environmental stability, and dispersibility and potentially imparting new properties by introducing foreign functional units onto nanomaterials.

In addition, screening PPy against the MXene space and aligning the possibilities to various applications using artificial intelligence AI algorithms and computational material techniques, such as density functional theory, will be an efficient method to adopt.

■ AUTHOR INFORMATION

Corresponding Author

Suprakas Sinha Ray − *Centre for Nanostructures and Advanced Materials, DSI-CSIR Nanotechnology Innovation Centre, Council for Scientific and Industrial Research, CSIR, Pretoria 0001, South Africa; Department of Chemical Sciences, University of Johannesburg, Doornfontein, Johannesburg 2028, South Africa;* orcid.org/0000-0002-0007-2595; Email: rsuprakas@csir.co.za

Authors

Gbolahan Joseph Adekoya − *Institute of Nanoengineering Research (INER) and Department of Chemical, Metallurgical and Materials Engineering, Faculty of Engineering and the Built Environment, Tshwane University of Technology, Pretoria 0001, South Africa; Centre for Nanostructures and Advanced Materials, DSI-CSIR Nanotechnology Innovation Centre, Council for Scientific and Industrial Research, CSIR, Pretoria 0001, South Africa*

Oluwasegun Chijioke Adekoya − *Institute of Nanoengineering Research (INER) and Department of Chemical, Metallurgical and Materials Engineering, Faculty of Engineering and the Built Environment, Tshwane University of Technology, Pretoria 0001, South Africa;* orcid.org/0000-0002-5386-5919

Rotimi Emmanuel Sadiku − *Institute of Nanoengineering Research (INER) and Department of Chemical, Metallurgical and Materials Engineering, Faculty of Engineering and the Built Environment, Tshwane University of Technology, Pretoria 0001, South Africa*

Yskandar Hamam − *Department of Electrical Engineering, Faculty of Engineering and the Built Environment, Tshwane University of Technology, Pretoria 0001, South Africa; École Supérieure d'Ingénieurs en Électrotechnique et Électronique, Cité Descartes, 93160 Noisy-le-Grand, Paris, France*

Complete contact information is available at:
https://pubs.acs.org/10.1021/acsomega.2c02706

Author Contributions

The manuscript was written with the contributions of all authors. GJA and SSR framed and organized the manuscript. RES edited and corrected the manuscript.

Notes

The authors declare no competing financial interest.

■ ACKNOWLEDGMENTS

■ REFERENCES

(1) Pomerantseva, E.; Bonaccorso, F.; Feng, X.; Cui, Y.; Gogotsi, Y. Energy storage: The future enabled by nanomaterials. *Science.* **2019**, *366* (6468), 969.

(2) Gogotsi, Y.; Penner, R. M. Energy storage in nanomaterials - capacitive, pseudocapacitive, or battery-like? *ACS Nano* **2018**, *12* (3), 2081−2083.

(3) Haastrup, S.; Strange, M.; Pandey, M.; Deilmann, T.; Schmidt, P. S.; Hinsche, N. F.; Gjerding, M. N.; Torelli, D.; Larsen, P. M.; Riis-Jensen, A. C.; Gath, J.; Jacobsen, K. W.; Jørgen Mortensen, J.; Olsen, T.; Thygesen, K. S. The computational 2D materials database: High-throughput modeling and discovery of atomically thin crystals. *2D Mater.* **2018**, *5* (4), 042002.

(4) Chakraborty, P.; Das, T.; Saha-Dasgupta, T. MXene: A New Trend in 2D Materials Science. In *Comprehensive Nanoscience and Nanotechnology*, 2nd ed.; Andrews, D. L., Lipson, R. H., Nann, T., Eds.; Acad. Press: Oxford, 2019; pp 319−330.

(5) Fang, R.; Lu, C.; Chen, A.; Wang, K.; Huang, H.; Gan, Y.; Liang, C.; Zhang, J.; Tao, X.; Xia, Y. 2D MXene-based energy storage materials: Interfacial structure design and functionalization. *ChemSusChem* **2019**, *6* (13), 1409−1419.

(6) Xiong, D.; Li, X.; Bai, Z.; Lu, S. Recent advances in layered $Ti_3C_2T_x$ MXene for electrochemical energy storage. *Small* **2018**, *14* (17), 1703419.

(7) Pang, J.; Mendes, R. G.; Bachmatiuk, A.; Zhao, L.; Ta, H. Q.; Gemming, T.; Liu, H.; Liu, Z.; Rummeli, M. H. Applications of 2D MXenes in energy conversion and storage systems. *Chem. Soc. Rev.* **2019**, *48* (1), 72−133.

(8) Jun, B.-M.; Kim, S.; Heo, J.; Park, C. M.; Her, N.; Jang, M.; Huang, Y.; Han, J.; Yoon, Y. Review of MXenes as new nanomaterials for energy storage/delivery and selected environmental applications. *Nano Res.* **2019**, *12* (3), 471−487.

(9) Zhang, X.; Zhang, Z.; Zhou, Z. MXene-based materials for electrochemical energy storage. *J. Energy Chem.* **2018**, *27* (1), 73−85.

(10) Anasori, B.; Lukatskaya, M. R.; Gogotsi, Y. 2D metal carbides and nitrides (MXenes) for energy storage. *Nature Rev. Mater.* **2017**, *2* (2), 1−17.

(11) Li, K.; Liang, M.; Wang, H.; Wang, X.; Huang, Y.; Coelho, J.; Pinilla, S.; Zhang, Y.; Qi, F.; Nicolosi, V.; Xu, Y. 3D MXene architectures for efficient energy storage and conversion. *Adv. Funct. Mater.* **2020**, *30* (47), 2000842.

(12) Gao, L.; Li, C.; Huang, W.; Mei, S.; Lin, H.; Ou, Q.; Zhang, Y.; Guo, J.; Zhang, F.; Xu, S.; Zhang, H. MXene/polymer membranes: Synthesis, properties, and emerging applications. *Chem. Mater.* **2020**, *32* (5), 1703−1747.

(13) Firouzjaei, M. D.; Karimiziarani, M.; Moradkhani, H.; Elliott, M.; Anasori, B. *MXenes: The two-dimensional influencers*; Elsevier: 2022; Vol. 13, p 100202.

(14) Tan, Z.-L.; Wei, J.-X.; Liu, Y.; Zaman, F. u.; Rehman, W.; Hou, L.-R.; Yuan, C.-Z. V_2CTx MXene and its derivatives: Synthesis and recent progress in electrochemical energy storage applications. *Rare Metals* **2022**, *41* (3), 775−797.

(15) Wang, Y.; Xu, Y.; Hu, M.; Ling, H.; Zhu, X. MXenes: Focus on optical and electronic properties and corresponding applications. *Nanophotonics* **2020**, *9* (7), 1601−1620.

(16) Griffith, K. J.; Hope, M. A.; Reeves, P. J.; Anayee, M.; Gogotsi, Y.; Grey, C. P. Bulk and surface chemistry of the niobium MAX and MXene phases from multinuclear solid-state NMR spectroscopy. *J. Am. Chem. Soc.* **2020**, *142* (44), 18924−18935.

(17) Aslam, M. K.; Niu, Y.; Xu, M. MXenes for non-lithium-ion (Na, K, Ca, Mg, and Al) batteries and supercapacitors. *Adv. Energy Mater.* **2021**, *11* (2), 2000681.

(18) Nan, J.; Guo, X.; Xiao, J.; Li, X.; Chen, W.; Wu, W.; Liu, H.; Wang, Y.; Wu, M.; Wang, G. Nanoengineering of 2D MXene-based materials for energy storage applications. *Small* **2021**, *17* (9), 1902085.

(19) Yang, Q.; Wang, Y.; Li, X.; Li, H.; Wang, Z.; Tang, Z.; Ma, L.; Mo, F.; Zhi, C. Recent progress of MXene-based nanomaterials in felexible energy storage and electronic devices. *Energy Environ. Mater.* **2018**, *1* (4), 183−195.

(20) Xiao, Z.; Li, Z.; Meng, X.; Wang, R. MXene-engineered lithium−sulfur batteries. *J. Mater. Chem. A* **2019**, *7* (40), 22730−22743.

(21) Michael, J.; Qifeng, Z.; Danling, W. Titanium carbide MXene: Synthesis, electrical and optical properties and their applications in sensors and energy storage devices. *Nanomater. Nanotechnol.* **2019**, *9*, 1−9.

(22) Sun, S.; Liao, C.; Hafez, A. M.; Zhu, H.; Wu, S. Two-dimensional MXenes for energy storage. *Chem. Eng. J.* **2018**, *338*, 27−45.

(23) Okada, Y.; Keilbart, N.; Goff, J. M.; Higai, S. i.; Shiratsuyu, K.; Dabo, I. MXene electrode materials for electrochemical energy storage:

First-principles and grand canonical Monte Carlo Simulations. *MRS Adv.* **2019**, *4* (33−34), 1833−1841.

(24) Fang, R.; Lu, C.; Chen, A.; Wang, K.; Huang, H.; Gan, Y.; Liang, C.; Zhang, J.; Tao, X.; Xia, Y.; Zhang, W. 2D MXene-based energy storage materials: Interfacial structure design and functionalization. *ChemSusChem* **2020**, *13* (6), 1409−1419.

(25) Chen, X.; Zhao, Y.; Li, L.; Wang, Y.; Wang, J.; Xiong, J.; Du, S.; Zhang, P.; Shi, X.; Yu, J. MXene/polymer nanocomposites: preparation, properties, and applications. *Polym. Rev.* **2021**, *61* (1), 80−115.

(26) Jimmy, J.; Kandasubramanian, B. Mxene functionalized polymer composites: Synthesis and applications. *Eur. Polym. J.* **2020**, *122*, 109367.

(27) Kim, S. Y.; Hong, J.; Palmore, G. T. R. Polypyrrole decorated cellulose for energy storage applications. *Synth. Met.* **2012**, *162* (15), 1478−1481.

(28) Brzózka, A.; Fic, K.; Bogusz, J.; Brudzisz, A. M.; Marzec, M. M.; Gajewska, M.; Sulka, G. D. Polypyrrole-nickel hydroxide hybrid nanowires as future materials for energy storage. *Nanomat.* **2019**, *9* (2), 307.

(29) Ates, M.; Caliskan, S.; Gazi, M. A ternary nanocomposites of graphene/TiO_2/polypyrrole for energy storage applications. *Fullerenes, Nanotubes Carbon Nanostruct.* **2018**, *26* (10), 631−642.

(30) Ahn, K.-J.; Lee, Y.; Choi, H.; Kim, M.-S.; Im, K.; Noh, S.; Yoon, H. Surfactant-templated synthesis of polypyrrole nanocages as redox mediators for efficient energy storage. *Sci. Rep.* **2015**, *5* (1), 14097.

(31) Arul, N. S.; Han, J. I. Polypyrrole nanostructures//activated carbon based electrode for energy storage applications. *J. Mater. Sci. Mater. Electron.* **2019**, *30* (8), 7890−7900.

(32) Jian, X.; He, M.; Chen, L.; Zhang, M.; Li, R.; Gao, L.; Fu, F.; Liang, Z. Three-dimensional carambola-like MXene/polypyrrole composite produced by one-step co-electrodeposition method for electrochemical energy storage. *Electrochim. Acta* **2019**, *318*, 820−827.

(33) Yan, J.; Ma, Y.; Zhang, C.; Li, X.; Liu, W.; Yao, X.; Yao, S.; Luo, S. Polypyrrole-MXene coated textile-based flexible energy storage device. *RSC Adv.* **2018**, *8* (69), 39742−39748.

(34) Wei, D.; Wu, W.; Zhu, J.; Wang, C.; Zhao, C.; Wang, L. A facile strategy of polypyrrole nanospheres grown on Ti_3C_2-MXene nanosheets as advanced supercapacitor electrodes. *J. Electroanal. Chem.* **2020**, *877*, 114538.

(35) Zhou, S.; Gu, C.; Li, Z.; Yang, L.; He, L.; Wang, M.; Huang, X.; Zhou, N.; Zhang, Z. $Ti_3C_2T_x$ MXene and polyoxometalate nanohybrid embedded with polypyrrole: Ultra-sensitive platform for the detection of osteopontin. *Appl. Surf. Sci.* **2019**, *498*, 143889.

(36) Ezika, A. C.; Sadiku, E. R.; Ray, S. S.; Hamam, Y.; Folorunso, O.; Adekoya, G. J. Emerging advancements in polypyrrole MXene hybrid nanoarchitectonics for capacitive energy storage applications. *J. Inorg. Organomet. Polym.* **2022**, *32* (5), 1521−1540.

(37) Ma, C.; Sg, P.; Pr, G.; Shashwati, S. Synthesis and characterization of polypyrrole (PPy) thin films. *Soft Nanosci. Lett.* **2011**, *2011* (1), 6.

(38) Sakthivel, S.; Boopathi, A. Synthesis and characterization of polypyrrole (PPy) thin film by spin coating Technique. *J. Chem. Chem. Sci.* **2014**, *4*, 150−155.

(39) Vernitskaya, T. y. V.; Efimov, O. N. Polypyrrole: A conducting polymer; its synthesis, properties and applications. *Russ. Chem. B+* **1997**, *66* (5), 443−457.

(40) Dey, S.; Kar, A. K. Morphological and optical properties of polypyrrole nanoparticles synthesized by variation of monomer to oxidant ratio. *Mater. Today: Proc.* **2019**, *18*, 1072−1076.

(41) Wang, Y.; Song, R.; Li, L.; Fu, R.; Liu, Z.; Li, B. High crystalline quality conductive polypyrrole film prepared by interface chemical oxidation polymerization method. *Appl. Sci.* **2022**, *12* (1), 58.

(42) Dianatdar, A.; Miola, M.; De Luca, O.; Rudolf, P.; Picchioni, F.; Bose, R. K. All-dry, one-step synthesis, doping and film formation of conductive polypyrrole. *J. Mater. Chem. C* **2022**, *10* (2), 557−570.

(43) Boota, M.; Anasori, B.; Voigt, C.; Zhao, M. Q.; Barsoum, M. W.; Gogotsi, Y. Pseudocapacitive electrodes produced by oxidant-free polymerization of pyrrole between the layers of 2D titanium carbide (MXene). *Adv. Mater.* **2016**, *28* (7), 1517−1522.

(44) Tan, Y.; Ghandi, K. Kinetics and mechanism of pyrrole chemical polymerization. *Synth. Met.* **2013**, *175*, 183−191.

(45) Camurlu, P. Polypyrrole derivatives for electrochromic applications. *RSC Adv.* **2014**, *4* (99), 55832−55845.

(46) Sadki, S.; Schottland, P.; Brodie, N.; Sabouraud, G. The mechanisms of pyrrole electropolymerization. *Chem. Soc. Rev.* **2000**, *29* (5), 283−293.

(47) Cao, J.; Han, Y.; Zheng, X.; Wang, Q. Preparation and electrochemical performance of modified $Ti_3C_2T_x$/polypyrrole composites. *J. Appl. Polym. Sci.* **2019**, *136* (4), 47003.

(48) Raagulan, K.; Kim, B. M.; Chai, K. Y. Recent advancement of electromagnetic interference (EMI) shielding of two dimensional (2D) MXene and graphene aerogel composites. *Nanomaterials* **2020**, *10* (4), 702.

(49) Naguib, M.; Mochalin, V. N.; Barsoum, M. W.; Gogotsi, Y. 25th anniversary article: MXenes: A new family of two-dimensional materials. *Adv. Mater.* **2014**, *26* (7), 992−1005.

(50) Nam, S.; Kim, J.-N.; Oh, S.; Kim, J.; Ahn, C. W.; Oh, I.-K. $Ti_3C_2T_x$ MXene for wearable energy devices: Supercapacitors and triboelectric nanogenerators. *APL Mater.* **2020**, *8* (11), 110701.

(51) Li, X.; Huang, Z.; Zhi, C. Environmental stability of MXenes as energy storage materials. *Front. Mater.* **2019**, *6*, 312.

(52) Ezika, A. C.; Sadiku, E. R.; Idumah, C. I.; Ray, S. S.; Adekoya, G. J.; Odera, R. S. Recently emerging trends in MXene hybrid conductive polymer energy storage nanoarchitectures. *Polym.-Plast Technol. Mater.* **2022**, *61* (8), 861−887.

(53) Shi, X.-y.; Gao, M.-h.; Hu, W.-w.; Luo, D.; Hu, S.-z.; Huang, T.; Zhang, N.; Wang, Y. Largely enhanced adsorption performance and stability of MXene through in-situ depositing polypyrrole nanoparticles. *Sep. Purif. Technol.* **2022**, *287*, 120596.

(54) Al-Shannaq, R.; Farid, M. M. 10 - Microencapsulation of phase change materials for thermal energy storage systems. In *Advances in Thermal Energy Storage Systems*, 2nd ed.; Cabeza, L. F., Ed.; Woodhead Publishing, 2021; pp 269−329.

(55) Seyedin, S.; Zhang, J.; Usman, K. A. S.; Qin, S.; Glushenkov, A. M.; Yanza, E. R. S.; Jones, R. T.; Razal, J. M. Facile solution processing of stable MXene dispersions towards conductive composite fibers. *Global Challenges* **2019**, *3* (10), 1900037.

(56) Liu, T.; Liu, N.; An, Q.; Xiao, Z.; Zhai, S.; Li, Z. Designed construction of $Ti_3C_2T_x$@PPY composites with enhanced microwave absorption performance. *J. Alloys Compd.* **2019**, *802*, 445−457.

(57) Zhu, M.; Huang, Y.; Deng, Q.; Zhou, J.; Pei, Z.; Xue, Q.; Huang, Y.; Wang, Z.; Li, H.; Huang, Q.; Zhi, C. Highly flexible, freestanding supercapacitor electrode with enhanced performance obtained by hybridizing polypyrrole chains with MXene. *Adv. Energy Mater.* **2016**, *6* (21), 1600969.

(58) Uyor, U. O.; Popoola, A. P.; Popoola, O.; Aigbodion, V. S. Energy storage and loss capacity of graphene-reinforced poly(vinylidene fluoride) nanocomposites from electrical and dielectric properties perspective: A review. *Adv. Polym. Technol.* **2018**, *37* (8), 2838−2858.

(59) Adekoya, G. J.; Sadiku, R. E.; Ray, S. S. Nanocomposites of PEDOT:PSS with graphene and its derivatives for flexible electronic applications: A review. *Macromol. Mater. Eng.* **2021**, *306* (3), 2000716.

(60) Zhang, X.; Li, J.; Li, J.; Han, L.; Lu, T.; Zhang, X.; Zhu, G.; Pan, L. 3D TiO_2@nitrogen-doped carbon/Fe_7S_8 composite derived from polypyrrole-encapsulated alkalized MXene as anode material for high-performance lithium-ion batteries. *Chem. Eng. J.* **2020**, *385*, 123394.

(61) Lei, Y.; Tan, N.; Zhu, Y.; Huo, D.; Sun, S.; Zhang, Y.; Gao, G. Synthesis of porous N-rich carbon/MXene from MXene@ polypyrrole hybrid nanosheets as oxygen reduction reaction electrocatalysts. *J. Electrochem. Soc.* **2020**, *167* (11), 116503.

(62) Li, X.; Hao, J.; Liu, R.; He, H.; Wang, Y.; Liang, G.; Liu, Y.; Yuan, G.; Guo, Z. Interfacing MXene flakes on fiber fabric as an ultrafast electron transport layer for high performance textile electrodes. *Energy Storage Mater.* **2020**, *33*, 62−70.

(63) Wu, W.; Wei, D.; Zhu, J.; Niu, D.; Wang, F.; Wang, L.; Yang, L.; Yang, P.; Wang, C. Enhanced electrochemical performances of organ-

like Ti$_3$C$_2$ MXenes/polypyrrole composites as supercapacitors electrode materials. *Ceram. Int.* **2019**, *45* (6), 7328−7337.

(64) Yang, D.; Zhou, B.; Han, G.; Feng, Y.; Ma, J.; Han, J.; Liu, C.; Shen, C. Flexible transparent polypyrrole-decorated MXene-based film with excellent photothermal energy conversion performance. *ACS Appl. Mater. Interfaces.* **2021**, *13* (7), 8909−8918.

(65) Le, T. A.; Tran, N. Q.; Hong, Y.; Lee, H. Intertwined titanium carbide MXene within a 3D tangled polypyrrole nanowires matrix for enhanced supercapacitor performances. *Chemistry* **2019**, *25* (4), 1037− 1043.

(66) Ding, J.; Tang, C.; Zhu, G.; He, F.; Du, A.; Wu, M.; Zhang, H. Ultrasmall SnO$_2$ nanocrystals sandwiched into polypyrrole and Ti$_3$C$_2$Tx MXene for highly effective sodium storage. *Mater. Chem. Front.* **2021**, *5* (2), 825−833.

(67) Shao, J.; Wang, J.-W.; Liu, D.-N.; Wei, L.; Wu, S.-Q.; Ren, H. A novel high permittivity percolative composite with modified MXene. *Polymer* **2019**, *174*, 86−95.

(68) Yildirim, E.; Goh, S. S.; Luo, H.-K.; Jin, H.; Wu, G.; Tan, T. L.; Wong, Z. M.; Xu, J.; Yang, S.-W. A dual-surface mechanism of oxidant-free pyrrole polymerization in the two-dimensional titanium carbide (MXene) interlayer nanospace. *J. Phys. Chem. C* **2022**, *126* (3), 1316− 1325.

(69) Zhang, C.; Xu, S.; Cai, D.; Cao, J.; Wang, L.; Han, W. Planar supercapacitor with high areal capacitance based on Ti$_3$C$_2$/Polypyrrole composite film. *Electrochim. Acta* **2020**, *330*, 135277.

(70) Song, Q.; Zhan, Z.; Chen, B.; Zhou, Z.; Lu, C. Biotemplate synthesis of polypyrrole@ bacterial cellulose/MXene nanocomposites with synergistically enhanced electrochemical performance. *Cellulose* **2020**, *27* (13), 7475−7488.

(71) Urbankowski, P.; Anasori, B.; Hantanasirisakul, K.; Yang, L.; Zhang, L.; Haines, B.; May, S. J.; Billinge, S. J. L.; Gogotsi, Y. 2D molybdenum and vanadium nitrides synthesized by ammoniation of 2D transition metal carbides (MXenes). *Nanoscale* **2017**, *9* (45), 17722− 17730.

(72) Liang, W.; Zhitomirsky, I. MXene-polypyrrole electrodes for asymmetric supercapacitors. *Electrochim. Acta* **2022**, *406*, 139843.

(73) Zou, H.; Wu, S.; Shen, J. Polymer/silica nanocomposites: Preparation, characterization, Properties, and applications. *Chem. Rev.* **2008**, *108* (9), 3893−3957.

(74) Goh, P. S.; Ismail, A. F.; Ng, B. C. Chapter 2 - Raman Spectroscopy. In *Membrane Characterization*; Hilal, N., Ismail, A. F., Matsuura, T., Oatley-Radcliffe, D., Eds.; Elsevier: 2017; pp 31−46.

(75) Jaleh, B.; Fakhri, P. Chapter 5 - Infrared and Fourier transform infrared spectroscopy for nanofillers and their nanocomposites. In *Spectroscopy of Polymer Nanocomposites*; Thomas, S., Rouxel, D., Ponnamma, D., Eds.; William Andrew Publishing: 2016; pp 112−129.

(76) You, Q.; Guo, Z.; Zhang, R.; Chang, Z.; Ge, M.; Mei, Q.; Dong, W.-F. Simultaneous recognition of dopamine and uric acid in the presence of ascorbic acid via an intercalated MXene/PPy nanocomposite. *Sensors* **2021**, *21* (9), 3069.

(77) Begum, B.; Bilal, S.; Shah, A. U.; Röse, P. Physical, chemical, and electrochemical properties of redox-responsive polybenzopyrrole as electrode material for Faradaic energy storage. *Polymers* **2021**, *13* (17), 2883.

(78) Wu, D.; Cheng, X.; Zhang, T.; Gao, H. Multifunctional MXene: Improve electromagnetic interference shielding of PPy/PDA/Ti$_3$C$_2$T$_x$ composites in X-and Ku-band. *Polym. Adv. Technol.* **2022**, *33* (6), 1898−1905.

(79) Sinha Ray, S.; Okamoto, M. Polymer/layered silicate nano-composites: A review from preparation to processing. *Prog. Polym. Sci.* **2003**, *28* (11), 1539−1641.

(80) Zha, X.-H.; Zhou, J.; Zhou, Y.; Huang, Q.; He, J.; Francisco, J. S.; Luo, K.; Du, S. Promising electron mobility and high thermal conductivity in Sc$_2$CT$_2$ (T = F, OH) MXenes. *Nanoscale* **2016**, *8* (11), 6110−6117.

(81) Shahzad, F.; Alhabeb, M.; Hatter, C. B.; Anasori, B.; Man Hong, S.; Koo, C. M.; Gogotsi, Y. Electromagnetic interference shielding with 2D transition metal carbides (MXenes). *Science* **2016**, *353* (6304), 1137.

(82) Elgrishi, N.; Rountree, K. J.; McCarthy, B. D.; Rountree, E. S.; Eisenhart, T. T.; Dempsey, J. L. A practical beginner's guide to cyclic voltammetry. *J. Chem. Educ.* **2018**, *95* (2), 197−206.

(83) Licht, F.; Davis, M. A.; Andreas, H. A. Charge redistribution and electrode history impact galvanostatic charging/discharging and associated figures of merit. *J. Power Sources* **2020**, *446*, 227354.

(84) Lv, J.; Liu, Z.; Zhang, L.; Li, K.; Zhang, S.; Xu, H.; Mao, Z.; Zhang, H.; Chen, J.; Pan, G. Multifunctional polypyrrole and rose-like silver flower-decorated E-textile with outstanding pressure/strain sensing and energy storage performance. *Chem. Eng. J.* **2022**, *427*, 130823.

(85) Yibowei, M. E.; Adekoya, J. G.; Adediran, A. A.; Adekomaya, O. Carbon-based nano-filler in polymeric composites for supercapacitor electrode materials: a review. *Environ. Sci. Pollut. Res.* **2021**, *28* (21), 26269−26279.

(86) Zhang, R.; Pang, H. Application of graphene-metal/conductive polymer based composites in supercapacitors. *J. Energy Storage* **2021**, *33*, 102037.

(87) Najam, T.; Shah, S. S. A.; Peng, L.; Javed, M. S.; Imran, M.; Zhao, M.-Q.; Tsiakaras, P. Synthesis and nano-engineering of MXenes for energy conversion and storage applications: Recent advances and perspectives. *Coord. Chem. Rev.* **2022**, *454*, 214339.

(88) Wang, W.; Xu, H.; Zhao, W.; Zhao, J.; Jiang, M.; Liu, S.; Huang, W.; Zhao, Q. Porphyrin-assisted synthesis of hierarchical flower-like polypyrrole arrays based flexible electrode with high areal capacitance. *Chem. Eng. J.* **2022**, *428*, 131089.

(89) Lukatskaya, M. R.; Kota, S.; Lin, Z.; Zhao, M.-Q.; Shpigel, N.; Levi, M. D.; Halim, J.; Taberna, P.-L.; Barsoum, M. W.; Simon, P.; Gogotsi, Y. Ultra-high-rate pseudocapacitive energy storage in two-dimensional transition metal carbides. *Nat. Energy* **2017**, *2* (8), 1−6.

(90) Du, C.-F.; Zhao, X.; Wang, Z.; Yu, H.; Ye, Q. Recent advanced on the MXene-organic hybrids: Design, synthesis, and their applications. *Nanomaterials* **2021**, *11* (1), 166.

(91) Kausar, A. Polymer/MXene nanocomposite-a new age for advanced materials. *Polym-Plast Technol. Mater.* **2021**, *60* (13), 1377− 1392.

(92) Pasha, A.; Khasim, S.; Darwish, A. A. A.; Hamdalla, T. A.; Al-Ghamdi, S. A.; Alfadhli, S. Flexible, stretchable and electrically conductive PDMS decorated with polypyrrole/manganese-iron oxide nanocomposite as a multifunctional material for high performance EMI shielding applications. *Syn. Met.* **2022**, *283*, 116984.

(93) Muhammed Anees, P. K.; Vannathan, A. A.; Abhijith, M. B.; Kella, T.; Shee, D.; Mal, S. S. Imidazolium cation linkers of polyoxomolybdate-polypyrrole nanocomposite electrode-based energy storage supercapacitors. *Mater. Chem. Phys.* **2022**, *277*, 125441.

(94) Feng, Y.; Zhang, M.; Yan, H.; Zhang, Y.; Guo, R.; Wang, H. Microwave-assisted efficient exfoliation of MXene and its composite for high-performance supercapacitors. *Ceram. Int.* **2022**, *48* (7), 9518− 9526.

(95) Shaikh, N. S.; Ubale, S. B.; Mane, V. J.; Shaikh, J. S.; Lokhande, V. C.; Praserthdam, S.; Lokhande, C. D.; Kanjanaboos, P. Novel electrodes for supercapacitor: Conducting polymers, metal oxides, chalcogenides, carbides, nitrides, MXenes, and their composites with graphene. *J. Alloys Compd.* **2022**, *893*, 161998.

(96) Vandana, M.; Veeresh, S.; Ganesh, H.; Nagaraju, Y. S.; Vijeth, H.; Basappa, M.; Devendrappa, H. Graphene oxide decorated SnO$_2$ quantum dots/polypyrrole ternary composites towards symmetric supercapacitor application. *J. Energy Storage* **2022**, *46*, 103904.

(97) Liu, X.; Zhu, S.; Liang, Y.; Li, Z.; Wu, S.; Luo, S.; Chang, C.; Cui, Z. 3D N-doped mesoporous carbon/SnO$_2$ with polypyrrole coating layer as high-performance anode material for Li-ion batteries. *J. Alloys Compd.* **2022**, *892*, 162083.

(98) Feng, Y.; Liu, H.; Lu, Q.; Liu, Y.; Li, J.; He, X.; Liu, X.; Mikhailova, D. Designing hierarchical MnO/polypyrrole heterostructures to couple polysulfides adsorption and electrocatalysis in lithium-sulfur batteries. *J. Power Sources* **2022**, *520*, 230885.

(99) Folorunso, O.; Hamam, Y.; Sadiku, R.; Ray, S. S.; Adekoya, G. J. Investigation of graphene loaded polypyrrole for lithium-ion battery. *Mater. Today: Proceedings* **2021**, *38*, 635−638.

(100) Folorunso, O.; Hamam, Y.; Sadiku, R.; Ray, S. S.; Adekoya, G. J. Synthesis methods of borophene, graphene-loaded polypyrrole nanocomposites and their benefits for energy storage applications: A brief overview. *FlatChem.* **2021**, *26*, 100211.

(101) Folorunso, O.; Hamam, Y.; Sadiku, R.; Ray, S. S.; Adekoya, G. J. Statistical characterization and simulation of graphene-loaded polypyrrole composite electrical conductivity. *J. Mater. Res. Technol.* **2020**, *9* (6), 15788−15801.

(102) Ghidiu, M.; Lukatskaya, M. R.; Zhao, M.-Q.; Gogotsi, Y.; Barsoum, M. W. Conductive two-dimensional titanium carbide 'clay' with high volumetric capacitance. *Nature* **2014**, *516* (7529), 78−81.

(103) Boota, M.; Gogotsi, Y. MXene—conducting polymer asymmetric pseudocapacitors. *Adv. Energy Mater.* **2019**, *9* (7), 1802917.

(104) Zhan, C.; Naguib, M.; Lukatskaya, M.; Kent, P. R. C.; Gogotsi, Y.; Jiang, D.-e. Understanding the MXene pseudocapacitance. *J. Phys. Chem. Lett.* **2018**, *9* (6), 1223−1228.

(105) Shinde, P. A.; Patil, A. M.; Lee, S.; Jung, E.; Chan Jun, S. Two-dimensional MXenes for electrochemical energy storage applications. *J.. Mater. Chem. A* **2022**, *10*, 1105−1149.

(106) Lu, C.; Xuan, J.; Min, H. E.; Mi-mi, Z.; Xiao-die, C.; Lou-jun, G. A. O.; Zhen-hai, L. Preparation and Capacitive Property of Two-Dimensional Multilayer $Ti_3C_2T_x$-MXene/PPy-NW Composite Material. *J. Electrochem.* **2019**, *25* (2), 280.

(107) Fan, Q.; Zhao, R.; Yi, M.; Qi, P.; Chai, C.; Ying, H.; Hao, J. Ti_3C_2-MXene composite films functionalized with polypyrrole and ionic liquid-based microemulsion particles for supercapacitor applications. *Chem. Eng. J.* **2022**, *428*, 131107.

(108) Das, P.; Wu, Z.-S. MXene for energy storage: present status and future perspectives. *J. Phys. Energy* **2020**, *2* (3), 032004.

(109) Li, X.; Zhu, J.; Liang, W.; Zhitomirsky, I. MXene (Ti_3C_2Tx) anodes for asymmetric supercapacitors with high active mass loading. *Mater. Chem. Phys.* **2021**, *268*, 124748.

(110) Li, X.; Ma, Y.; Shen, P.; Zhang, C.; Cao, M.; Xiao, S.; Yan, J.; Luo, S.; Gao, Y. An ultrahigh energy density flexible asymmetric microsupercapacitor based on Ti_3C_2Tx and PPy/MnO_2 with wide voltage window. *Adv. Mater. Technol.* **2020**, *5* (8), 2000272.

(111) Ma, C.; Ma, M.-G.; Si, C.; Ji, X.-X.; Wan, P. Flexible MXene-based composites for wearable devices. *Adv. Funct. Mater.* **2021**, *31* (22), 2009524.

(112) Wang, Q.; Song, H.; Li, W.; Wang, S.; Liu, L.; Li, T.; Han, Y. Facile synthesis of polypyrrole/graphene composite aerogel with Alizarin Red S as reactive dopant for high-performance flexible supercapacitor. *J. Power Sources* **2022**, *517*, 230737.

(113) Tumacder, D. V.; Morávková, Z.; Bober, P. Enhanced electrochemical performance of electrosynthesized fibrillar polypyrrole film. *Mater. Lett.* **2022**, *308*, 131295.

(114) Shi, X.; Sun, L.; Li, X.; Wu, L.; Qian, J.; Wang, J.; Lin, Y.; Su, S.; Sun, C.; Zhang, Y.; Zhang, Y. High-performance flexible supercapacitor enabled by Polypyrrole-coated NiCoP@CNT electrode for wearable devices. *J. Colloid Interface Sci.* **2022**, *606*, 135−147.

(115) Yang, L.; Lin, F.; Zabihi, F.; Yang, S.; Zhu, M. High specific capacitance cotton fiber electrode enhanced with PPy and MXene by in situ hybrid polymerization. *Int. J. Biol. Macromol.* **2021**, *181*, 1063−1071.

(116) Vaghasiya, J. V.; Mayorga-Martinez, C. C.; Vyskočil, J.; Pumera, M. Flexible wearable MXene Ti_3C_2-Based power patch running on sweat. *Biosens. Bioelectron.* **2022**, *205*, 114092.

(117) Li, J.; Chen, J.; Wang, H.; Xiao, X. All-MXene cotton-based supercapacitor-powered human body thermal management system. *ChemElectroChem.* **2021**, *8* (4), 648−655.

(118) Jost, K.; Durkin, D. P.; Haverhals, L. M.; Brown, E. K.; Langenstein, M.; De Long, H. C.; Trulove, P. C.; Gogotsi, Y.; Dion, G. Natural fiber welded electrode yarns for knittable textile supercapacitors. *Adv. Energy Mater.* **2015**, *5* (4), 1401286.

(119) Zhang, W.; Jin, H.; Zhang, J. Nb_2CT_x MXene as high-performance energy storage material with Na, K, and liquid K-Na alloy anodes. *Langmuir* **2021**, *37* (3), 1102−1109.

(120) Mahajan, M.; Singla, G.; Ogale, S. Polypyrrole-encapsulated polyoxomolybdate decorated MXene as a functional 2D/3D nano-hybrid for a robust and high performance Li-ion battery. *ACS Appl. Energy Mater.* **2021**, *4* (5), 4541−4550.

(121) Li, L.; Xu, J.; Shi, M.; He, J.; Jiang, J.; Dai, K.; Jiang, Z.; Yan, C. In-situ Raman investigation and application of MXene-stabilized polypyrrole composite for flexible aqueous batteries. *Mater. Des.* **2022**, *217*, 110606.

(122) Wen, Y.; He, K.; Zhu, Y.; Han, F.; Xu, Y.; Matsuda, I.; Ishii, Y.; Cumings, J.; Wang, C. Expanded graphite as superior anode for sodium-ion batteries. *Nat. Commun.* **2014**, *5* (1), 4033.

(123) Kim, S.-W.; Seo, D.-H.; Ma, X.; Ceder, G.; Kang, K. Electrode materials for rechargeable sodium-ion batteries: Potential alternatives to current lithium-ion batteries. *Adv. Energy Mater.* **2012**, *2* (7), 710−721.

(124) Slater, M. D.; Kim, D.; Lee, E.; Johnson, C. S. Sodium-ion batteries. *Adv. Funct. Mater.* **2013**, *23* (8), 947−958.

(125) Yabuuchi, N.; Kubota, K.; Dahbi, M.; Komaba, S. Research development on sodium-ion batteries. *Chem. Rev.* **2014**, *114* (23), 11636−11682.

(126) Hwang, J.-Y.; Myung, S.-T.; Sun, Y.-K. Sodium-ion batteries: present and future. *Chem. Soc. Rev.* **2017**, *46* (12), 3529−3614.

(127) Huang, Y.; Li, K.; Liu, J.; Zhong, X.; Duan, X.; Shakir, I.; Xu, Y. Three-dimensional graphene/polyimide composite-derived flexible high-performance organic cathode for rechargeable lithium and sodium batteries. *J. Mater. Chem. A* **2017**, *5* (6), 2710−2716.

(128) Peng, H.; Wang, S.; Kim, M.; Kim, J.; Yamauchi, Y.; Yu, J.; Li, D. Highly reversible electrochemical reaction of insoluble 3D nanoporous polyquinoneimines with stable cycle and rate performance. *Energy Storage Mater.* **2020**, *25*, 313−323.

(129) Liu, H.; Wang, J.-G.; Hua, W.; Ren, L.; Sun, H.; Hou, Z.; Huyan, Y.; Cao, Y.; Wei, C.; Kang, F. Navigating fast and uniform zinc deposition via a versatile metal-organic complex interphase. *Energy Environ. Sci.* **2022**, *15* (5), 1872−1881.

(130) Zhang, Y.; Cao, Z.; Liu, S.; Du, Z.; Cui, Y.; Gu, J.; Shi, Y.; Li, B.; Yang, S. Charge-enriched strategy based on MXene-based polypyrrole layers toward dendrite-free zinc metal anodes. *Adv. Energy Mater.* **2022**, *12* (13), 2103979.

(131) Wang, C.-C.; Wei, S.-C.; Luo, S.-C. Recent advances and biomedical applications of peptide-integrated conducting polymers. *ACS Appl. Bio Mater.* **2022**, *5* (5), 1916−1933.

(132) Bettucci, O.; Matrone, G. M.; Santoro, F. Conductive polymer-based bioelectronic platforms toward sustainable and biointegrated devices: A journey from skin to brain across human body interfaces. *Adv. Mater. Technol.* **2022**, *7* (2), 2100293.

(133) Dinu, A.; Apetrei, C. A review of sensors and biosensors modified with conducting polymers and molecularly imprinted polymers used in electrochemical detection of amino acids: Phenylalanine, tyrosine, and tryptophan. *Int. J. Mol. Sci.* **2022**, *23* (3), 1218.

(134) Ratautaite, V.; Boguzaite, R.; Brazys, E.; Ramanaviciene, A.; Ciplys, E.; Juozapaitis, M.; Slibinskas, R.; Bechelany, M.; Ramanavicius, A. Molecularly imprinted polypyrrole based sensor for the detection of SARS-CoV-2 spike glycoprotein. *Electrochim. Acta* **2022**, *403*, 139581.

(135) Qu, K.; Qiu, Y.; Li, J. Electro-catalytic behavior by polypyrrole-derived carbon supported iron for simultaneous electrochemical sensing of dopamine and uric acid. *J. Electroanal. Chem.* **2022**, *910*, 116188.

(136) Cai, Y.; Shen, J.; Yang, C.-W.; Wan, Y.; Tang, H.-L.; Aljarb, A. A.; Chen, C.; Fu, J.-H.; Wei, X.; Huang, K.-W.; et al. Mixed-dimensional MXene-hydrogel heterostructures for electronic skin sensors with ultrabroad working range. *Sci. Adv.* **2020**, *6* (48), No. eabb5367.

(137) Chen, P.; Zhao, Z.; Shao, Z.; Tian, Y.; Li, B.; Huang, B.; Zhang, S.; Liu, C.; Shen, X. Highly selective NH_3 gas sensor based on polypyrrole/$Ti_3C_2T_x$ nanocomposites operating at room temperature. *J. Mater. Sci. Mater. Electon.* **2022**, *33* (9), 6168−6177.

(138) Tong, Y.; He, M.; Zhou, Y.; Zhong, X.; Fan, L.; Huang, T.; Liao, Q.; Wang, Y. Hybridizing polypyrrole chains with laminated and two-dimensional $Ti_3C_2T_x$ toward high-performance electromagnetic wave absorption. *Appl. Surf. Sci.* **2018**, *434*, 283−293.

(139) Babayan, V.; Kazantseva, N. E.; Moučka, R.; Stejskal, J. Electromagnetic shielding of polypyrrole-sawdust composites: polypyrrole globules and nanotubes. *Cellulose* **2017**, *24* (8), 3445−3451.

(140) Ramoa, S. D. A. S.; Barra, G. M. O.; Merlini, C.; Livi, S.; Soares, B. G.; Pegoretti, A. Electromagnetic interference shielding effectiveness and microwave absorption properties of thermoplastic polyurethane/ montmorillonite-polypyrrole nanocomposites. *Polym. Adv. Technol.* **2018**, *29* (5), 1377−1384.

(141) Keskinen, J.; Tuurala, S.; Sjödin, M.; Kiri, K.; Nyholm, L.; Flyktman, T.; Strømme, M.; Smolander, M. Asymmetric and symmetric supercapacitors based on polypyrrole and activated carbon electrodes. *Synth. Met.* **2015**, *203*, 192−199.

(142) Wen, X.; Zhang, Q.; Guan, J. Applications of metal-organic framework-derived materials in fuel cells and metal-air batteries. *Coord. Chem. Rev.* **2020**, *409*, 213214.